

FINAL REPORT

**Stability of U(VI) and Tc(VII) Reducing Microbial Communities to Environmental
Perturbation: Development and Testing of a Thermodynamic Network Model**

Project ID: 0011072

Principal Investigator:

Jonathan D. Istok

Owen Hall 220

Department of Civil Engineering

Oregon State University

Corvallis, Oregon 97331

Jack.Istok@orst.edu: 541-737-8547

June 1, 2008

PROJECT SUMMARY

‘Bioimmobilization’ of redox-sensitive metals and radionuclides is being investigated as a way to remediate contaminated groundwater and sediments. In this approach, growth-limiting substrates are added to stimulate the activity of targeted groups of indigenous microorganisms and create conditions favorable for the microbially-mediated precipitation (‘bioimmobilization’) of targeted contaminants. This project investigated a fundamentally new approach for modeling this process that couples thermodynamic descriptions for microbial growth with associated geochemical reactions. In this approach, a synthetic microbial community is defined as a collection of defined microbial groups; each with a growth equation derived from bioenergetic principles. The growth equations and standard-state free energy yields are appended to a thermodynamic database for geochemical reactions and the combined equations are solved simultaneously to predict the effect of added substrates on microbial biomass, community composition, and system geochemistry. This approach, *with a single set of thermodynamic parameters* (one for each growth equation), was used to predict the results of laboratory and field bioimmobilization experiments at two geochemically diverse research sites. Predicted effects of ethanol or acetate addition on uranium and technetium solubility, major ion geochemistry, mineralogy, microbial biomass and community composition were in general agreement with experimental observations although the available experimental data precluded rigorous model testing. Model simulations provide insight into the long-standing difficulty in transferring experimental results from the laboratory to the field and from one field site to the next, especially if the form, concentration, or delivery of growth substrate is varied from one experiment to the next. Although originally developed for use in better understanding bioimmobilization of uranium and technetium via reductive precipitation, the modeling approach is potentially useful

for exploring the coupling of microbial growth and geochemical reactions in a variety of basic and applied biotechnology research settings.

INTRODUCTION

The oxidized and mobile forms of uranium and technetium (such as uranyl carbonates or pertechnetate) have been shown to undergo microbially-mediated reductive transformations that result in the formation of less soluble products that are also less mobile in the environment. For example, certain anaerobic bacteria can enzymatically reduce $U^{(VI)}$ to $U^{(IV)}$, which is essentially insoluble and, when sorbed, aggregated into large particles, or deposited onto sediment mineral phases, is also immobile (e.g., Lovley et al., 1993). Similarly, by stimulating the bio-reduction of technetium, it is possible to decrease aqueous concentrations of the mobile pertechnetate ion ($Tc^{(VII)}O_4^-$) by forming insoluble and immobile $Tc^{(IV)}$ -oxides or sulfides (e.g., Wildung et al., 2000). Thus, by stimulating targeted indigenous microbial activities, aqueous concentrations and the migration of uranium and technetium will be decreased. Analogous 'bioimmobilization' processes are possible for other redox-sensitive metals and radionuclides including Cr, V, and Pu (http://www.lbl.gov/ERSP/generalinfo/primers_guides/03_NABIR_primer.pdf). Although organisms with the capability to reduce $U^{(VI)}$ and $Tc^{(VII)}$ are apparently widespread in the subsurface, their activity is often limited by relatively small numbers, the availability of a suitable electron donor, high concentrations of competing electron acceptors, the presence of potential growth inhibitors, and perhaps other site-specific factors. Moreover, other groups of microorganisms and certain chemical processes are capable of reoxidizing (and thus remobilizing) $U^{(IV)}$ and $Tc^{(IV)}$, (Senko et al. 2005a,b) and the rates of these processes need to be controlled so that aqueous uranium and technetium concentrations remain small.

In field experiments, bioimmobilization of uranium and technetium has been shown to involve the growth and metabolic activity of a diverse group of microorganisms including aerobes, denitrifiers, manganese reducers, iron reducers, sulfate reducers, and methanogens;

important geochemical parameters include relative concentrations of oxygen, nitrate, and sulfate and the quantity and bioavailability of $\text{Fe}^{(\text{III})}$ and $\text{Mn}^{(\text{IV})}$ -bearing mineral phases (Anderson et al., 2003; Istok et al., 2004; Vrionis et al., 2005; Wu et al., 2006a,b). Although much has been learned about the physiology and metabolic potential of pure cultures of microorganisms with the ability to reduce $\text{U}^{(\text{VI})}$ and $\text{Tc}^{(\text{VII})}$ (Lovley et al., 1993; Jain et al., 1997; Chandler et al., 1997; Wildung et al., 2000; Fredrickson et al., 2000; Coates et al., 2001; Payne et al., 2002), major gaps exist in our understanding of the functioning of these organisms when they are embedded in an intact microbial community, where competition, syntrophy, and complementary catabolic pathways are defining characteristics. Although these relationships have been long addressed in macrocommunity ecology (MacArthur and Wilson, 1967; Tilman, 1982; Hubbel, 2001), very little research has been directed toward quantifying these relationships for microbial communities.

Most pristine subsurface environments, and even many contaminated ones, are oligotrophic, having insufficient carbon or other nutrients to support sustained microbial growth (Williams, 1985; Ghiorse and Wilson, 1988; Kieft et al., 1994). Natural fluctuations in resource availability typically result in short periods of rapid growth followed by longer periods with greatly reduced rates of metabolism (Muller et al., 2002). By contrast, in engineered systems, supplies of carbon or other nutrients are typically much larger and are controlled (along with other process variables) in an attempt to create a modified microbial community that can sustain the highest possible rates of material flows (e.g. as related to waste water treatment, industrial biomass/biochemical production, etc.) (Smith and McCarty, 1990). For example, to create conditions favorable for uranium and technetium bioimmobilization at the Department of Energy's Field Research Center at Oak Ridge National Laboratory,

several additions of electron donor at concentrations up to 300 mM were required, and these caused major shifts in rates of microbial activity, viable biomass, and community composition (Peacock et al., 2003; North et al., 2004; Brodie et al., 2006; Michalsen et al. 2007).

The current ‘state-of-the-art’ in bioimmobilization research typically utilizes an empirical approach to select the type and concentrations of exogenous substrates required to stimulate growth of the targeted microorganisms (typically iron- or sulfate-reducing bacteria). As an interesting example, acetate additions were used to stimulate $U^{(VI)}$ reduction at a field site in Rifle, CO (Anderson et al., 2003, Vrionis et al., 2005, Yabusaki et al 2007). At that site, $U^{(VI)}$ reduction was observed until shifts in microbial community composition allowed sulfate-reducing bacteria to out-compete iron reducing bacteria for added acetate, at which point $U^{(VI)}$ reduction slowed or ceased. In contrast, ethanol was more effective than acetate in stimulating $U^{(VI)}$ and $Tc^{(VII)}$ reduction at a field site in Oak Ridge, TN (Istok et al., 2004), and the reduction of $U^{(VI)}$, $Fe^{(III)}$, $Mn^{(IV)}$, and sulfate were observed to proceed concomitantly. Large differences in the geochemical environment at the two sites (including pH and initial concentrations of nitrate and sulfate) and differences in experimental configuration (method of substrate delivery and spatial and temporal scales) also likely contributed to differences in observed system responses to substrate addition at the two sites. This suggests that a more comprehensive theoretical framework is needed to predict and interpret the effects of substrate addition on microbial community composition and contaminant geochemistry. Such a framework would also be potentially useful for synthesizing results obtained from different experimental configurations (laboratory batch vs. column experiments, field push-pull tests vs. natural gradient tests, etc.) and

for transferring findings from small-scale laboratory and field studies to full-scale field implementation.

Energy and material flows in an intact microbial community are coupled to an extensive network of geochemical reactions and processes (acid/base reactions, mineral precipitation and dissolution reactions, sorption and cation exchange reactions, etc.) that can affect the energy and biomass yields and the kinetics of microbial growth processes (Fredrickson et al., 1998; Zachara et al., 1998; Zachara et al., 2001; Kostka et al., 2002; Benner et al., 2002). In particular, research has shown that responses of the microbial community to exogenous substrate additions can be very different in geochemical environments that can have greatly different concentrations of potential soluble and mineral-associated electron acceptors. This can be an important issue in contaminated environments, which are typically geochemically complex. For example, at the Department of Energy's Field Research Center (FRC) at Oak Ridge National Laboratory, groundwater pH varies from ~ 3 to 8, nitrate concentrations range from 0 to over 200 mM, and sulfate concentrations range from 0 to ~ 10 mM (Istok et al., 2004; Wu et al., 2006a,b), while uranium and technetium are present at much lower concentrations (nM to μM). Moreover, geochemical processes control the solubility and bioavailability of $\text{Fe}^{(\text{III})}$ and $\text{Mn}^{(\text{IV})}$ -bearing mineral phases and the aqueous concentrations of Fe^{2+} and Mn^{2+} . For example, research has shown that as Fe^{2+} accumulates, rates of $\text{Fe}^{(\text{III})}$ - and $\text{U}^{(\text{VI})}$ -reduction slow (Wielinga et al., 2000; Royer et al., 2004). However, in sulfate rich environments, HS^- produced by sulfate-reducing bacteria can combine with Fe^{2+} and precipitate as various mineral phases, thus removing potentially inhibitory Fe^{2+} from solution (Abdelouas et al., 2002). Other research has emphasized the role of manganese oxides in

the reduction of $\text{Fe}^{(\text{III})}$, $\text{U}^{(\text{VI})}$, and $\text{Tc}^{(\text{VII})}$ (Fredrickson et al., 2002) as well as the abiotic reduction of metals and radionuclides by reduced mineral phases (Cui and Eriksen, 1996; O'Loughlin et al., 2003; McKinley et al., 2002). Clearly, an accurate assessment of exogenous substrate addition on microbial growth and community composition must include a system-specific coupling between microbial growth and system geochemistry.

Perhaps the most widely used approach for modeling microbial growth has been to use Monod-type kinetic expressions to describe rates of substrate utilization and biomass production (Banwart and Thornton, 2003). A variety of kinetic models have been successfully used to describe data from laboratory and field experiments and have yielded important insights into how microbial processes control material and energy flows in natural and engineered systems (Van Capellen and Wang, 1996; Beyenal et al., 2001; Ginn et al., 2001; Yeh et al., 2001a,b; Liu et al., 2001; Burgos et al., 2002; Yabusaki et al., 2007). Perhaps their greatest utility has been in understanding the patterns and rates of substrate utilization by pure or mixed cultures in laboratory microcosms (Watson et al., 2003) or in more complex engineered systems such as anaerobic waste water digesters (Mosey and Fernandes, 1989; Smith and McCarty, 1990; McCarty and Mosey, 1991). It should be noted that other types of kinetic models have been developed in an attempt to describe in detail the metabolism of an individual organism (Reed and Palsson, 2003), and a pure culture (Savinell and Palsson, 1992) and may ultimately be extended to describe the behavior of entire microbial communities (as suggested by Schilling et al., 1999).

However, kinetic models have a number of limitations that justify the exploration of alternative approaches for modeling microbial community dynamics. For example, for simplicity some models assume that biomass remains constant during periods of substrate utilization, which is clearly unrealistic when substrate inputs are large. In addition, some models

do not explicitly couple microbial activity with geochemical reactions that affect the energy available for growth. Also, kinetic models may assume that microbial activity at any point in space or time is controlled by a single dominant terminal electron accepting process (TEAP), which is inconsistent with laboratory and field studies that clearly show that, when substrate inputs are large, multiple TEAPs can be active simultaneously (e.g., Bjerg et al., 1995). But perhaps the most important limitation of the kinetic modeling approach is that it requires values for a large number of system-specific rate parameters and obtaining these is currently problematic because of the well-known difficulties (1) in estimating multiple, perhaps statistically correlated kinetic parameters from available growth data (e.g., Liu and Zachara, 2001), (2) in applying laboratory-derived kinetic parameters to complex and heterogeneous natural systems (e.g., Nuttmann et al., 2005), (3) in applying kinetic parameters obtained from one experimental configuration to a different one (e.g. Jin and Bethke, 2003), and (4) in scaling parameters obtained in small-scale laboratory experiments to larger-scale field experiments (e.g., Schirmer et al., 2003). It is therefore unlikely that kinetic models will have true predictive power until new methods for obtaining model parameters are developed and validated. This is particularly important as model descriptions of microbial communities become more complex and require an ever increasing number of kinetic parameters.

To complement existing kinetic modeling efforts, we are developing and testing an alternative modeling technique for predicting microbial growth that couples two, well-known theoretical approaches developed in different disciplines. The first is the ‘bioenergetics’ approach widely used to predict biomass yield in various biotechnology fields (e.g., Battley, 1987; Heijen and van Dijken, 1991; Rittmann and McCarty, 2001). The second is the thermodynamic equilibrium modeling approach used to describe the chemical speciation of

natural water/sediment systems in geochemistry (e.g., Bethke, 1996). The modeling approach presented here uses thermodynamic principals from bioenergetics to predict the system-specific, free energy available for microbial growth in a particular environment by simultaneously solving a coupled system of microbial growth equations and ‘abiotic’ geochemical reactions using well-know techniques of thermodynamic equilibrium modeling widely used in geochemistry. This approach ignores the kinetics of microbial growth and geochemical processes and thus is not capable of predicting microbial growth or geochemical composition as a function of time and in fact, allows for a variety of system responses during the period of ‘kinetic control’ that immediately follows the addition of a growth-limiting substrate (Fig. 1). However, we postulate that, for many applications, the detailed temporal response of the microbial community may be less important than the ‘final’ state of the system (e.g., the biomass and community composition and resulting system geochemistry after added substrate is consumed and energy sources available for growth are again small), which is ultimately controlled by thermodynamics (Fig. 1). It should also be recognized that, compared to time scales involved in field-scale bioimmobilization strategies for redox-sensitive metals and radionuclides (~ years to decades and longer), the duration of the period of kinetic ‘control’ may be relatively small (~hours to days) so that thermodynamic considerations may dominate long-term system response, although this conjecture remains untested.

In the modeling approach presented here, the intact, indigneous microbial community (containing potentially many thousands of species, many uncharacterized) is represented as a set of defined microbial groups. All organisms in each group obtain energy by catalyzing a single redox reaction and producing biomass according to a specified growth equation with fixed stoichiometry and biomass yield, with one growth equation per group. For each increment of

added substrate consumed, the set of growth equations and a parallel set of ‘abiotic’ geochemical reactions are solved simultaneously to obtain quantitative predictions for the increase in biomass for all groups, the resulting community composition, and the effects of growth on contaminant and major ion geochemistry and mineralogy. Of course, essential features of any modeling approach are that (1) model parameters should be measurable, and (2) model predictions should be testable. Fortunately, as we will show, an important advantage of our approach is that the number of adjustable model parameters is very small (much smaller than comparable kinetic modeling approaches), which greatly simplifies the description of complex microbial communities in diverse geochemical environments. Also, the continued development of molecular biological tools for characterizing the composition of complex microbial communities is providing additional capabilities for testing model predictions. Nevertheless, it is recognized that the use of thermodynamics to predict microbial growth involves many assumptions, discussed in the next section, most of which have not been rigorously tested in complex natural environments.

In a series of examples, the proposed modeling approach, *with a single set of parameters derived a priori from the literature*, was used to predict the results of laboratory and field experiments conducted at two geochemically diverse, contaminated research sites. *No iterative parameter estimation was performed to improve the fit between model predictions and experimental observations.* Remarkably, model predictions for the effects of ethanol and acetate additions on microbial biomass and community composition, uranium and technetium concentrations and speciation, major ion geochemistry, and sediment mineralogy were in general, although largely qualitative, agreement with laboratory and field experiments.

However important technological difficulties in verifying model predictions remain and these will be discussed in the context of the specific experiments.

MODEL DEVELOPMENT

Microbial Groups and Growth Equations. Intact microbial communities from any natural environment are complex and comprised of perhaps thousands of species, most of which have not been characterized and whose members cannot all be detected or quantified with existing technologies. Thus, the species-level models widely used in macrocommunity ecology (e.g. Roughgarden et al., 1989) are difficult to apply to microbial communities. Instead, for modeling purposes we define a *synthetic microbial community* as a collection of defined *microbial groups*, each containing organisms with a common metabolic capability. Our use of the term ‘microbial group’ is similar but not identical to the terms ‘guild’ and ‘respiratory guild’, which are typically used to refer to a collection of specific species that use a particular resource in the same way (e.g., Fraterrigo et al., 2005). Instead, in our approach, a microbial group is defined as the collection of all organisms that have the capability to catalyze a particular oxidation-reduction reaction involving defined pairs of organic and/or inorganic substrates. It is recognized that this approach represents a severe simplification of the diverse physiology of microorganisms in nature, and that many specific microorganisms share overlapping metabolic capabilities. Moreover, modeling an intact microbial community as a finite set of distinct microbial groups will always be problematic because most microorganisms are capable of dealing with changes in their environment by existing in different physiological states, and by shifting from one state to another as conditions change (e.g., Karthikeyan et al., 1999). Nevertheless, as we will show in the examples, the proposed modeling approach appears to

capture many qualitative and quantitative features of microbial growth and shifting community composition observed in several experiments performed in extremely complex geochemical environments.

For the simulations presented below we selected microbial groups to reflect the major metabolic capabilities identified in experiments aimed at stimulating indigenous microbial activity in radionuclide contaminated environments at the two research sites (described below) where these processes have been studied in detail (Anderson et al., 2003; Vrionis et al. 2005, Istok et al., 2004; North et al., 2004; Wu et al., 2006a,b; Michalsen et al., 2006, 2007). These include organisms that can couple oxygen, nitrate, sulfate, $\text{Fe}^{(\text{III})}$, $\text{Mn}^{(\text{IV})}$, $\text{U}^{(\text{VI})}$, and $\text{Tc}^{(\text{VII})}$ reduction to the complete or partial oxidation of ethanol, acetate, or hydrogen, and methanogens for a total of 28 groups (Table 1). (Of course, it would be possible to define other microbial groups using other metabolic activities required to describe other systems). Once, the groups are defined, growth equations (one per microbial group) are derived using well-established ‘bioenergetics’ principles (e.g., Battley, 1987; Heijnen, 1991; Rittmann and McCarty, 2001). Rittmann and McCarty (2001) presented procedures for deriving growth equations by coupling a pair of energy-yielding redox half-reactions with an equation for cell synthesis so that overall reactions for microbial growth can be written:

$$R_i = f_{e_i} R_{a_i} + f_{s_i} R_{c_i} - R_{d_i} \quad (1)$$

where R_i is the overall growth equation for group i , f_{e_i} is the portion of transferred electrons used for energy production, f_{s_i} is the portion of transferred electrons used for cell synthesis ($f_{e_i} + f_{s_i} = 1$), R_{a_i} is the electron acceptor half-reaction, R_{c_i} is the synthesis reaction, and R_{d_i} is the electron donor half-reaction. In this approach, growth equations can be derived once the adjustable

parameters (fe_i or fs_i) that partition energy obtained by electron donor oxidation between maintenance and growth are specified.

In another approach, Heijnen (1991) presented procedures for deriving growth equations by solving a system of simultaneous equations that include elemental balances, conservation of charge, and conservation of energy. The energy balance equations are written using the Gibbs free energy of formation for each chemical species and a term that describes the ‘Gibbs energy dissipated per C-mol produced biomass’, which Heijnen and Dijken (1991) gave the symbol D_s^{01}/r_{Ax} . If D_s^{01} is the rate of Gibbs energy dissipation during growth ($\text{kJ/m}^3 \text{ h}$) and r_{ax} is the growth rate ($\text{C-mol/m}^3 \text{ h}$) then D_s^{01}/r_{Ax} is the Gibbs energy that must be dissipated to produce 1C-mol of biomass from the available carbon source, nitrogen source, electron donor, and electron acceptor.

For our simulations, growth equations were derived using a combination of Rittmann and McCarty (2001) and Heijnen (1991) approaches to derive the growth equations and thermodynamic data from the literature (e.g. Thauer et al., 1977). In every case, growth equations were set up by combining half reactions for biomass synthesis from ammonia and bicarbonate/organic compound, electron donor oxidation and electron acceptor reduction. The formula for biomass is $\text{CH}_x\text{N}_y\text{O}_z$ and was not included in each column of the table, but was included in the formulae and was set at 1 mol per equation. D_s^{01}/r_{Ax} values were obtained from Heijnen et al. (1992). For incorporation into existing geochemical thermodynamic databases it is convenient to write the growth equations in the form:

$$\begin{aligned} 1\text{C-mol Biomass} = & v_1 (\text{NH}_4^+) + v_2 (\text{H}^+) + v_3 (\text{H}_2\text{O}) + v_4 (\text{HCO}_3^-) \\ & + v_5 (\text{electron donor}) + v_6 (\text{electron acceptor}) + v_7 (\text{other}) = 0 \end{aligned} \quad (2)$$

where v_1 - v_7 are stoichiometric coefficients (positive or negative), and “other” refers to a metabolic product (e.g., N_2 , Fe^{2+} , Mn^{2+} , HS^- , acetate, H_2 , UO_2 , etc.). The biomass yield, Y_{DX} , which is defined as the C-mol of produced biomass per amount of electron donor consumed (C-mol for organic donors or mol for inorganic donors), was derived from the growth equation and is also tabulated in Table 1; values for Y_{DX} ranged from 0.01 to 0.56 and were generally largest for aerobes, denitrifiers, and manganese reducers and smallest for iron reducers, sulfate reducers, syntrophs, and methanogens.

Is important to emphasize that the growth equations were derived using a single set of adjustable parameters (one parameter per growth equation for a total of 28) either fs_i used in the Ritmann and McCarty (2001) approach or D_s^{01}/r_{AX} used in the Hiejnen (1991) approach. Clearly, the accuracy of growth predictions will be limited, in part, by the accuracy of these parameters, which were typically derived from laboratory growth experiments using pure cultures, completely mixed batch reactors, and relatively large cell densities. Moreover, it is important to recognize that the amount of biomass produced is also strongly influenced by the supply of potential electron acceptors, which, in the experiments discussed below, varied over a much wider range (~ 1 nM to 0.2 M) than Y_{DX} , suggesting that, in many situations, the accuracy of growth predictions may be more sensitive to uncertainties in initial electron acceptor concentrations than to uncertainties in selected values for fs_i or D_s^{01}/r_{AX} . This is particularly true for $U^{(VI)}$ and $Tc^{(VII)}$, which are typically present at three or more orders of magnitude smaller concentration than the other soluble electron acceptors. Alternatively, perhaps the largest uncertainty in simulations presented below may be the initial quantities of $Fe^{(III)}$ - and $Mn^{(IV)}$ -bearing mineral phases and the relative bioavailability of $Fe(III)$ and $M(IV)$, which are typically only poorly constrained by

existing sediment characterization data and are likely more uncertain than the growth parameters for iron- and manganese-reducing microbial groups.

Note that although we have elected to define microbial groups with the capability to directly (i.e. enzymatically) reduce $U^{(VI)}$ and $Tc^{(VII)}$, the extremely low initial aqueous concentrations of these contaminants (~ 0.4 nM to ~ 5 μ M) compared to other electron acceptors (200 μ M to 200 mM), limit the growth of these organisms compared to other groups. Also, it is recognized that growth via $Tc^{(VII)}$ reduction may not occur in natural environments and, instead, $Tc^{(VII)}$ may be reduced abiotically by $Fe^{(II)}$ (e.g., produced by the growth of iron reducing bacteria) (Lloyd et al., 2000). However, our modeling approach can readily accommodate either mechanism for $Tc^{(VII)}$ reduction and, because initial Tc concentrations were so small (~ 1 nM), essentially identical predicted patterns of microbial growth, community composition, and geochemical evolution will be predicted for either mechanism.

Coupling Microbial Growth Equations and Geochemical Reactions. The standard-state free energy change involved in producing 1C-mol of biomass, ΔG_r^0 (Table 1) for each growth equation was computed using:

$$\Delta G_r^0 = \sum_{i=1}^n \Delta G_{f,i}^0 v_i \quad (3)$$

where $\Delta G_{f,i}^0$ and v_i are the standard-state free energy of formation and stoichiometric coefficient for each chemical species in the growth equation. Computed values for ΔG_r^0 ranged from -24671 to +22,343 kJ/mol. It is important to recognize that although values for ΔG_r^0 tabulated in Table 1 were computed using *standard-state* (i.e. molar concentrations of aqueous species, etc., see e.g., Drever, 1992) free energies of formation

for reactants and products, at each point in the simulation the actual concentrations of reactants and product are used to calculate the system-specific free energy for each growth reaction and to determine if microbial growth of any group is possible.

The standard-state free energy change of the growth reactions is typically entered into thermodynamic databases as the natural logarithm of the equilibrium reaction constant, logK:

$$\log K = -\frac{\Delta G_r^\circ}{RT} \quad (9)$$

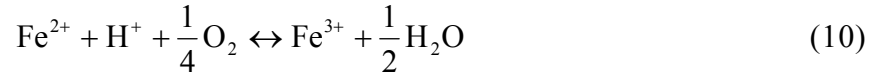
where R is the universal gas constant and T is the absolute temperature. Computed values for logK are in Table 1 and ranged from -3914 to 4322.

The growth equations and logK values for each microbial group were appended to a thermodynamic database for abiotic reactions developed at Lawrence Livermore National Laboratory (the LLNL database; Delany and Lundeen, 1989), which has been widely used to model the geochemistry of natural water/sediment systems. We also appended the database with thermodynamic data for ethanol as an aqueous species using data from Madigan et al. (1997). The modified LLNL database is available on request from the corresponding author. It is important to recognize that the chemical species in the growth equations also appear in one or more of the ‘abiotic’ geochemical reactions and this provides the principal couplings between microbiology and geochemistry in our modeling approach.

Reaction Path Calculations. Simulations were performed using a commercial geochemical reaction modeling software package, The Geochemist’s Work Bench (GWB) (Bethke, 1996) but similar calculations could be performed with one of several other widely-available software packages (e.g. MINTEQA, PHREEQ, and others listed in Bethke, 1996). Given

a defined initial geochemical environment (chemical composition of porewater and sediment minerals, temperature, etc.), GWB calculates the equilibrium mass distribution among aqueous species and mineral phases using well known thermodynamic principles (e.g. Bethke, 1996). By appending the microbial growth equations to the thermodynamic database, GWB can similarly calculate the equilibrium mass distribution among aqueous species, mineral phases, and biomass in each microbial group.

Several important issues arise when modeling microbial growth using geochemical reaction modeling software. The first involves redox coupling. The LLNL data bases contain a set of redox couples involving pairs of aqueous species such as $\text{Fe}^{3+}/\text{Fe}^{2+}$, $\text{SO}_4^{2-}/\text{HS}^-$, and so on, each defined by a coupling reaction that is balanced in terms of an electron donor or acceptor. For example, the redox coupling reaction for the $\text{Fe}^{3+}/\text{Fe}^{2+}$ couple is:



The redox coupling reactions force mathematical dependence between the computed concentrations of each member of the redox couple (e.g Fe^{3+} and Fe^{2+}). This is in conflict with the growth equations for (in this case) the iron reducer groups, where aqueous Fe^{3+} concentrations are controlled by the solubility of $\text{Fe}^{(\text{III})}$ -bearing mineral phases and Fe^{2+} concentrations are controlled, in part, by the supply of electron donor for growth, thus creating a condition of “redox disequilibrium”. To avoid this conflict, we “decoupled” (disallowed) the redox coupling equations for all redox species appearing in the growth equations (Table 1), namely: $\text{CH}_3\text{COO}^-/\text{HCO}_3^-$, $\text{CH}_4/\text{HCO}_3^-$, $\text{Fe}^{3+}/\text{Fe}^{2+}$, H_2/H^+ , H_2/O_2 , $\text{HS}^-/\text{SO}_4^{2-}$, $\text{MnO}_4^-/\text{Mn}^{2+}$, $\text{MnO}_4^{2-}/\text{Mn}^{2+}$, N_2/NO_3^- , $\text{NH}_4^+/\text{NO}_3^-$, $\text{NO}_2^-/\text{NO}_3^-$, $\text{U}^{3+}/\text{U}^{4+}$, $\text{UO}_2^+/\text{U}^{4+}$,

$\text{UO}_2^{2+}/\text{U}^{4+}$, $\text{Tc}^{3+}/\text{TcO}_4^-$, $\text{TcO}_2^+/\text{TcO}_4^-$, $\text{TcO}_4^{2-}/\text{TcO}_4^-$, and $\text{TcO}_4^{3-}/\text{TcO}_4^-$. With these exceptions all other reactions in the LLNL database were active during the simulations.

The second issue is that simulations were performed for a highly simplified initial geochemical system consisting of water, various aqueous species, a single $\text{Fe}^{(\text{III})}$ -bearing mineral phase and a single $\text{Mn}^{(\text{IV})}$ -bearing mineral phase (of course additional mineral phases, aqueous complexes, etc. formed as a result of microbial growth and various geochemical reactions). *In particular, no reactive solid surfaces were included in the thermodynamic database and thus no aqueous:mineral surface reactions such as ion exchange, sorption, or surface complexation were allowed.* This was done because parameters required to parameterize such surfaces (surface area, surface charge, reaction site density, etc.) were not available for the sediments used in the experiments discussed below. Excluding these reactions influenced simulations in several ways. First, experimentally determined initial concentrations for soluble electron acceptors (e.g. O_2 , NO_3^- , SO_4^{2-} , $\text{U}^{(\text{VI})}$) were obtained by aqueous sampling and analysis and likely underestimated the total initial supply of these solutes in the subsurface (due to the association of some solutes with the solid phase due to sorption, diffusion-limited mass transfer from immobile water or trapped gas bubbles, or other factors). This may be particularly unrealistic for $\text{U}^{(\text{VI})}$ reducing groups because at the two field sites, most uranium is thought to be associated with the solid phase (Anderson et al. 2003; Wu et al., 2006a,b). Thus by using only measured aqueous concentrations it is likely that simulations likely underpredicted the growth of some groups.

The third issue that arises concerns the form and reactivity of $\text{Fe}(\text{III})$ - and $\text{Mn}(\text{IV})$ -bearing mineral phases, which are important factors in the growth of iron- and manganese

reducing bacteria, respectively. Because quantitative assays for the mineral assemblages in the sediments used in the various experiments were not available it was assumed that the initial ‘bioavailable’ $\text{Fe}^{(\text{III})}$ and $\text{Mn}^{(\text{IV})}$ (operationally determined by chemical extraction) were present as goethite [$\text{Fe}^{(\text{III})}\text{OOH}$] and pyrolusite [$\text{Mn}^{(\text{IV})}\text{O}_2$], respectively. Many studies have addressed the bioavailability and biomass yield of iron- and manganese-reducing organisms under various growth conditions including varying initial amounts and forms of mineral oxides (Kostka et al., 2002). Nevertheless, for these simulations goethite and pyrolusite were selected because they are the most thermodynamically stable mineral phases under the conditions of the experiments discussed below. It would of course be possible to specify alternate initial mineral assemblages but, under the assumption of geochemical equilibrium used in these simulations, these would react to form goethite and pyrolusite unless the formation of these minerals was “suppressed” or disallowed. For simplicity, we elected to allow all thermodynamically possible mineral phases in the simulations presented here. We are currently investigating the effect of initial mineral assemblages on resulting microbial community composition and these will be presented in a subsequent study.

A related issue is the fate of microbially generated Fe^{2+} , Mn^{2+} , and HS^- . As discussed above, no reactive mineral surfaces were included in the simulations and thus aqueous concentrations of all microbially-generated species were ultimately limited by the solubility of various mineral phases. In the simulations presented in the next section the most stable Fe^{2+} -, Mn^{2+} -, and HS^- -bearing mineral phases were typically magnetite [$(\text{Fe}^{(\text{III})}, \text{Fe}^{(\text{II})})_2\text{O}_4$], rhodocrosite [$\text{Mn}^{(\text{II})}\text{CO}_3$], and pyrite [$\text{Fe}^{(\text{II})}\text{S}_2$], respectively (although there were some exceptions as discussed in the examples). It is also known that Fe^{2+} and Mn^{2+}

produced by iron- and manganese reducing organisms can be strongly associated (e.g. sorbed) with mineral surfaces (especially iron oxide surfaces) and this could reduce the amount of bioavailable $\text{Fe}^{(\text{III})}$ and $\text{Mn}^{(\text{IV})}$ over the course of a simulation and lead to decreased predicted growth. As stated above we elected to exclude reactive mineral surfaces from our model. Thus, the entire supply of initial goethite and pyrolusite were assumed to be bioavailable. Similarly, accumulation of Fe^{2+} and Mn^{2+} could potentially reduce the free energy for growth of iron and manganese reducers, but in these simulations the solubility of Fe^{2+} and Mn^{2+} were controlled at relatively low concentrations by the solubility of magnetite, etc.

For the simulations presented below we computed equilibrium reaction paths (using the GWB program REACT) by incrementally adding small amounts of growth substrate (ethanol or acetate in these examples) to a defined geochemical system with an initial composition selected to match the conditions for each experiment at each site (Table 2). Reaction paths were constructed using both ‘batch’ and ‘flush’ modeling options in REACT. The ‘batch’ simulations are simple titrations and approximate those occurring in a completely mixed batch reactor in the laboratory but which also may apply to certain types of field tests (i.e. the ‘push-pull’ tests used by Istok et al., 2004). In batch simulations growth substrate is added incrementally to a closed (no mass transfer) sediment/water system with known initial composition. The ‘flush’ simulations are also titrations but in an open system and approximate those occurring in laboratory column experiments and natural gradient field tests. In flush simulations both growth substrate and unreacted porewater are added incrementally to a sediment/water system with known

initial composition. The added porewater displaces reacted porewater (but not minerals or biomass) from the system, which no longer participates in subsequent reactions.

In both batch and flush simulations the microbial community composition changes continuously along the reaction path reflecting (1) the varying concentrations of potential electron acceptors, electron donors, reduced products, and other geochemical variables, and (2) the stoichiometry of the growth equations and geochemical reactions. It is convenient to describe the specific geochemical environment at each point along the reaction path as a '*thermodynamic niche*'. Thus, any microbial group that can obtain energy for growth in a particular thermodynamic niche will grow, while other groups will not. Moreover, those groups that can obtain the most energy from growth in a particular thermodynamic niche will 'out-compete' other groups for the added growth substrate. Coupling between the 28 growth equations and the large set of abiotic geochemical reactions occurs through microbially-mediated donor oxidation and CO₂ production, H⁺ consumption, the reductive dissolution of Fe^(III)- and Mn^(IV)-bearing minerals, the precipitation of various hydroxide and carbonate minerals due to rising pH or HCO₃⁻ concentration, the precipitation of Fe^(II)-, Mn^(II)-, and HS⁻- bearing minerals, the reductive precipitation of U^(IV)- and Tc^(IV)-bearing minerals, and decreasing redox potential. Collectively, all of these processes can lead to complex system behavior as shown in the next section.

Simulations were performed using geochemical data compiled from analyses performed on groundwater and sediment samples from Areas 1 and 2 at the DOE's Field Research Center (FRC) at Oak Ridge National Laboratory and from the Old Rifle Uranium Mill Tailings Remedial Action (UMTRA) field site in Colorado (Table 2). Although

geochemical characteristics at both sites are spatially heterogeneous, the geochemical data used in the simulations were selected to be broadly representative of the initial contaminant and geochemical data for experiments reported by Anderson et al. (2003), Istok et al. (2004), and Michalsen et al. (2006, 2007). However, it is recognized that the accuracy of initial geochemical data is a clearly an important factor limiting the accuracy of model predictions. In particular it is important to note that, in many experiments, the initial chemical composition of the sediment was not well characterized and the amount and mineralogy of initial Fe^(III)- and Mn^(IV)-bearing minerals was often poorly constrained by the available data due to limited sampling, heterogeneity of subsurface conditions, variability in analytical methodology, and several other factors.

FRC Area 1 is characterized by low initial pH and very high initial nitrate and dissolved metals; FRC Area 2 is characterized by a more moderate pH and much lower initial nitrate with a roughly equal amount of sulfate. Compared to other potential electron acceptors concentration of U (~μM) and Tc (~nM) are very small in both areas. Old Rifle is characterized by circumneutral pH, smaller initial nitrate and higher initial sulfate than at the FRC, small initial U concentration, no Tc, and a small amount of V, which is a redox sensitive metal that is less mobile when reduced, analogous to U and Tc. V^(V) reduction was observed during field experiments at Old Rifle and has been shown to be mediated by iron reducing bacteria (Ortiz-Bernad et al., 2004). However, in these simulations we elected to ignore growth via V^(V) reduction as there is considerable uncertainty in the chemical speciation of vanadium in groundwater at the Old Rifle site and this precluded our developing realistic growth equations for this process. However, abiotic V^(V) reduction was considered, and in any event, the very low initial vanadium

concentration at Old Rifle means that growth via $V^{(V)}$ reduction would contribute negligible biomass to overall community growth and composition (similar to the negligible growth supported by $Tc^{(VII)}$ reduction at the FRC). Ethanol was added as an electron donor in laboratory and field experiments at the FRC; acetate was added as an electron donor in field experiments at Old Rifle.

It is important to note that all simulations presented here were performed with the same growth equations in Table 1, no iterative adjustment of model parameters was used to improve agreement of model predictions and experimental observations. The only differences between the simulations were that input variables were changed to reflect the varying initial geochemical conditions in the various laboratory and field experiments at the two sites (Table 2), the type and concentration of added electron donor, and the choice of “batch” or “flush” configuration for the reaction paths calculations.

RESULTS

Overview

Computed reaction paths show the resulting change in microbial biomass and community composition and geochemistry that occur following each incremental addition of acetate (experiments at Old Rifle) or ethanol (experiments at the FRC). Each point on the reaction path is characterized by a specific combination of geochemical parameters (e.g. pH, concentrations of potential electron acceptors, metabolic products, and other dissolved species, and specific amounts of each solid mineral phase) and these define the energy available for growth of each microbial group. Thus, at each point along the reaction path, i.e. within each ‘thermodynamic niche’ defined by the geochemical environment, those groups that can obtain energy for growth increase in numbers, depleting the supply of electron acceptors and producing metabolic

products that can accumulate (e.g., N_2), participate in other growth or geochemical reactions (e.g. H^+ , HS^- , $Fe(II)$, and CO_2), or serve as electron donors for other microbial groups (e.g, acetate and H_2). In these simulations, the growth sequence of microbial groups roughly parallels the usual TEAP sequence; initial increments of added growth substrate are utilized by aerobes, manganese reducers, and denitrifiers, while subsequent additions are utilized by sulfate-, $Fe^{(III)}$ -, $U^{(VI)}$ -, and $Tc^{(VII)}$ -reducers, and methanogens. However, there were several important differences between the sites, mainly with respect to differences in relative amounts of high-initial-concentration electron acceptors (esp. nitrate, sulfate, $Fe^{(III)}$, and $Mn^{(IV)}$). In particular, these differences influenced the differential growth of microbial groups that produce acetate and H_2 (e.g $Mn^{(IV)}$ reducers, sulfate reducers, and syntrophs) which played an important role in supporting growth of several groups

FRC Area 2

Batch Simulations. ‘Batch’ simulations predicted that ethanol addition will result in the growth of 13 of the 28 microbial groups in the database. These were combined for plotting purposes as follows (electron acceptor)(electron donor) half-reactions for each group from Table 1 shown in parentheses): ‘aerobes’ (O_2/H_2O)(H_2/H^+) and (O_2/H_2O)(CH_4/CO_2); ‘manganese reducers’ (MnO_4^-/Mn^{2+})(Acetate/ CO_2) and (MnO_4^-/Mn^{2+})(H_2/H^+); ‘denitrifiers’ (NO_3^-/N_2)(Ethanol/ CO_2); ‘sulfate reducers’ (SO_4^{2-}/HS^-)(Ethanol/Acetate); ‘iron reducers’ (Fe^{3+}/Fe^{2+})(H_2/H^+) and (Fe^{3+}/Fe^{2+})(Acetate/ CO_2); ‘syntrophs’; (H^+/H_2)(Ethanol/Acetate); ‘methanogens’ (CO_2/CH_4)(Acetate/ CO_2) and (CO_2/CH_4)(H_2/H^+); ‘uranium reducers’ (UO_2^{2+}/U^{4+})(Acetate/ CO_2); and ‘technetium reducers’ (TcO_4^-/TcO^{2+})(Acetate/ CO_2) (Figure 2). Growth of the remaining groups in Table 1 is not energetically favorable under these conditions. Interestingly, the

majority of growth for all groups occurred using the products of ethanol oxidation (acetate or H_2) as the electron donors rather than ethanol.

Simulations showed the increasing biomass and changing community composition that occurred as increasing amounts of ethanol were reacted (Figure 2). Early on in the reaction path, growth was dominated by manganese-reducers, iron-reducers, and denitrifiers, with much smaller growth of other groups, reflecting the relatively larger initial amounts of $Mn^{(IV)}$ - and $Fe^{(III)}$ bearing minerals and nitrate compared to oxygen and sulfate. As additional ethanol was reacted, growth of other groups became energetically favorable, especially methanogens and syntrophs. Patterns of growth of the various groups along the reaction path were reflected in a changing community composition. Growth of manganese- and iron-reducers accounted for > 75 % of the predicted biomass increase for the first 25 mmol/kg ethanol reacted. Further along the reaction path, as available $Mn^{(IV)}$ and $Fe^{(III)}$ were gradually depleted, the relative proportions (but not absolute biomass) of those groups decreased so that by the end of the reaction path they accounted for ~ 50 % of the total. At the end of the reaction path methanogens and syntrophs were the only groups that could continue to obtain energy for growth in this closed system.

Patterns of predicted growth and community composition were closely coupled to and affected substantial changes in the geochemical environment (Figure 2). Oxygen and nitrate were consumed early on the reaction path and sulfate was consumed after ~ 20 mmol/kg of ethanol was reacted. Growth of manganese- and iron-reducers resulted in the predicted complete dissolution of goethite and pyrolusite, the production of Fe^{2+} and Mn^{2+} , and the precipitation of magnetite [$(Fe^{(III)}, Fe^{(II)})_2O_4$] and rhodocrosite [$Mn^{(II)}CO_3$], respectively. Pyrite [$Fe^{(II)}S_2$] precipitated due to microbial production of Fe^{2+} and HS^- . Bicarbonate was produced as ethanol and acetate were oxidized to CO_2 , however, bicarbonate concentrations and pH were also

controlled by the solubility of various mineral phases, in particular, rhodocrosite, which precipitated due to microbial production of Mn^{2+} . Growth of aerobes, denitrifiers, and manganese reducers resulted in a drop in redox potential (plotted as pe). Growth of uranium- and technetium reducers, although contributing negligible biomass, resulted in the bioimmobilization of uranium and technetium; soluble $\text{U}^{(\text{VI})}$ was reduced and precipitated as uraninite [$\text{U}^{(\text{IV})}\text{O}_2$] and soluble $\text{Tc}^{(\text{VII})}$ was reduced and precipitated with microbially produced HS^- as technetium sulfide [$\text{Tc}^{(\text{IV})}_2\text{S}_7$]. As supplies of the more energetically favorable electron acceptors were depleted, growth of methanogens led to the accumulation of methane. It is interesting to note that although acetate and H_2 are important electron donors in this system, their concentration remains low at $< 10^{-6}$ mmol/kg throughout the reaction path as has been observed in natural settings (Lovley et al., 1994; Park et al., 2006).

Comparison to experimental data. Batch simulations were compared to data from a laboratory microcosm experiment (Mohanty et al., 2007) conducted using a sediment:water slurry prepared by combining 125 g of Area 2 sediment with 500 mL groundwater in a closed glass bottle. Microbial activity was stimulated by the addition of ~ 9 mM ethanol and monitored by periodic sampling. It is important to remember that in these and all subsequent simulations, microbial growth, community composition, and geochemical composition were predicted assuming thermodynamic equilibrium and the complete consumption of each increment of added electron donor without any consideration of the time required for these reactions to occur. Thus, aqueous concentrations of added ethanol are precisely zero at each point along the reaction path. However, experimental data were collected as a function of time following ethanol addition. Thus, to plot experimental data on the simulated reaction paths it was first necessary to compute the cumulative (i.e., from the start of the experiment) quantity of electron donor consumed at the

time of each sampling using the initial electron donor concentration and the measured electron donor concentrations during the experiment.

Batch simulations were in general agreement with experimental data, although sampling frequency, analytical detection limits, and analytical protocols prevented a rigorous comparison (Figure 3). Simulated and measured pHs were identical. Predicted decreases in nitrate and sulfate concentrations were observed, although the model predicted larger concentration decreases at smaller quantities of reacted ethanol than were observed in the experiment. Predicted increases in HCO_3^- and CH_4 , resulting from microbial donor oxidation and growth of methanogens, and predicted decreases in aqueous $\text{U}^{(\text{VI})}$, due to growth of uranium reducers were close to experimental observations. Moreover, model simulations for loss of $\text{Fe}^{(\text{III})}$ and accumulation of $\text{Fe}^{(\text{II})}$ and the precipitation and accumulation of $\text{U}^{(\text{IV})}$ as uraninite were very close to measured amounts of $\text{Fe}^{(\text{III})}$, $\text{Fe}^{(\text{II})}$, and $\text{U}^{(\text{IV})}$ obtained by sequential extraction of sediment samples collected during the experiment. It should be noted the mineralogy of sediment-associated $\text{Fe}^{(\text{II})}$ and $\text{U}^{(\text{IV})}$ was not determined in these experiments.

Model simulations predicted an increase in total biomass of $\sim 3.5 \times 10^7$ cells/gram consisting primarily of denitrifiers, iron reducers, and sulfate reducers, with an increasing percentage of methanogens and syntrophs as more ethanol was reacted (Figure 4). Slurry samples were collected periodically during the experiment and analyzed for total biomass and community composition using phospholipid fatty acid (PLFA) analyses and clone libraries. There was no significant difference between predicted total biomass and total biomass estimated from total PLFA content (assuming 2.5×10^4 cells/pmol PLFA and 10^{12} cells/gram of biomass) (Figure 4). Note that the standard deviation for PLFA biomass (estimated from triplicate PLFA analyses) was $\sim 7 \times 10^7$ cells/gram. Microbial community composition as measured by

constituent PLFA profiles changed after ethanol addition and contained PLFA indicative of nitrate, iron and sulfate reducing bacteria, consistent with model predictions. For example, growth of iron reducers and sulfate reducers were indicated by the presence of diagnostic PLFAs (16:1w7c and 18:1w7c for *Geobacter* sp. and 10Me16:0, cy17:0, cy19:0, i17:0 for *Desulfobacter* and *Desulfovibrio* sp.. However, PLFA data alone are unable to detect and quantify predicted growth of the various microbial groups.

A more complete description of changing microbial community composition during the experiment was provided by clone libraries prepared from selected slurry samples (Figure 4). These results confirmed predicted growth of iron reducing organisms (*Geobacter metallireducens* and other *Geobacters* as well as *Anaeromyxobacter*), which constituted up to 50 % of the total community composition early in the experiment, decreasing to approximately 25 % at the end of the reaction path, similar to model predictions. *Geobacter* and *Anaeromyxobacter* are also known uranium reducing organisms (Lovley et al., 1991; Wu et al., 2006) although model simulations predict only negligible growth via $U^{(VI)}$ reduction because initial uranium concentrations were so small. Clone libraries also detected the growth of denitrifying and sulfate reducing organisms predicted by the model.

Flush simulations. ‘Flush’ simulations for the same initial geochemical system predicted very different patterns of growth and microbial community composition than those predicted for the ‘batch’ simulations (Figure 5). Recall that in flush simulations, unreacted porewater is added with each increment of added electron donor, displacing reacted porewater (but not cells or minerals) from the system. In flush simulations larger amounts of biomass are produced for each reacted increment of electron donor compared to batch simulations because of the continuous influx of soluble electron acceptors (esp. nitrate and sulfate) into the system. In particular, the

growth of denitrifiers dominated predicted community composition during flush simulations because of the relatively high nitrate concentration in unreacted pore water and the relatively high biomass yield from denitrification compared to manganese reducers, iron reducers, and methanogens (e.g., $Y_{DX} = 0.27$ to 0.41 for denitrification and $Y_{DX} = 0.12$ to 0.29 for iron and manganese reduction, Table 1). In the batch simulations, growth of many groups eventually ceased as the fixed initial supplies of soluble electron acceptors were gradually depleted. In the flush simulations, however, the continued addition of soluble electron acceptors with each addition of unreacted porewater supported the continued growth of several microbial groups. Early on the reaction path, manganese reducers grew until available $Mn^{(IV)}$ was completely reduced, which occurred after ~ 14 mmol/kg ethanol were reacted. Growth of iron reducers then occurred until all available $Fe^{(III)}$ was reduced. However, growth of groups utilizing soluble electron acceptors occurred continuously throughout the reaction path, reflecting the varying concentrations of oxygen, nitrate, and sulfate in unreacted porewater added with each increment of ethanol. Interestingly, growth of syntrophs contributed substantial biomass throughout the reaction path and produced acetate and H_2 that supported the growth of aerobes, denitrifiers, sulfate reducers, and iron reducers. Predicted community compositions at each point of the reaction path were substantially different for the flush and batch simulations (Figures 2 and 5). Flush simulations predicted more total growth and larger and increasing proportions of aerobes, denitrifiers, sulfate reducers, and syntrophs, but smaller proportions of methanogens than predicted for the batch simulations.

As in the batch simulations, patterns of predicted microbial growth in the flush simulations were closely coupled to predicted changes in the geochemical environment (Figure 5). For example, growth of manganese reducers and iron reducers resulted in the dissolution of

pyrolusite and goethite although a larger amount of reacted ethanol was required before goethite was dissolved in the flush simulations compared to the batch simulations. Magnetite, calcite, rhodocrosite, and pyrite precipitated due to microbial production of Fe^{2+} , CO_2 , Mn^{2+} , and HS^- . It is interesting to note that calcite precipitation predicted in the flush simulations was not predicted in the batch simulations. Growth of uranium- and technetium reducers and methanogens resulted in the precipitation of uraninite and technetium sulfide, although this required larger amounts of reacted ethanol in the flush simulations than in the batch simulations. Technetium sulfide accumulated linearly while uraninite accumulated nonlinearly reflecting the varying solubility and mobility of various aqueous Tc and U species in reacted porewater flushed from the system. Methanogenesis was predicted to occur later in the reaction path in the flush simulations than in the batch simulations and, unlike the batch simulations, methane reached a predicted steady-state concentration rather than continuing to increase, reflecting the balance between microbial methane production and methane removal as reacted porewater was displaced from the system.

Comparison to experimental data. Flush simulations were compared to data from a long-term (408 days) column experiment conducted at the FRC by Michalsen et al. (2006). In that study, two large columns (15 cm diameter x 213 cm length) were packed with ~ 70 kg uncontaminated site sediment and continuously perfused with site groundwater containing ~ 0.8 mM NO_3^- , 4 μM U, 1 mM SO_4^{2-} , and 580 pM. Ethanol was injected daily to stimulate microbial growth and porewater samples were routinely collected from sampling ports distributed along the column length. During the experiment, 1450 L (~ 80 pore volumes) of groundwater were passed through the column and 18.1 mol of EtOH, 0.77 μmol Tc, 6.0 mmol U, 0.94 mol nitrate, and 1.2 mol sulfate were removed. After the last sampling event, eight sediment samples were collected for microbial community and geochemical characterization. Detailed experimental procedures and

complete geochemical and microbiological results are summarized in Michalsen et al. 2006 and Michalsen et al. 2007.

Flush simulations predicted the complete reduction of oxygen, nitrate, and sulfate due to growth of aerobes, denitrifiers, and sulfate reducers (Figure 7). Predicted growth of iron and manganese reducers led to the complete dissolution of goethite and pyrolusite and the precipitation of $\text{Fe}^{(\text{II})}$ and $\text{Mn}^{(\text{II})}$ as magnetite, siderite, and rhodocrosite while predicted growth of sulfate reducers led to the precipitation of pyrite. Predicted growth of uranium and technetium reducers led to the accumulation of uraninite and technetium sulfide and predicted growth of methanogens and syntrophs led to the production and accumulation of CH_4 and H_2 . The simulations compared favorably with experimental results reported by Michalsen et al.: “technetium concentrations decreased from ~ 580 to ~ 0 pM, nitrate decreased from 0.4 to 0 mM, uranium decreased from 4 to 0.1 μM , and sulfate decreased from 0.8 to 0 mM ... and “methane (~ 1 mM)...was detected in porewater ...mid-way through the experiment”. They also report measured loss of $\text{Fe}^{(\text{III})}$ and accumulation of $\text{Fe}^{(\text{II})}$ and the presence of iron sulfide in sediment samples detected by variable-temperature Mossbauer spectroscopy and “that the Mössbauer spectrum of an acid stable black precipitate collected from the stimulated sediment samples gave a doublet signal with spectral parameters similar to those of pyrite, which indicated presence of FeS_x species”. $\text{U}^{(\text{IV})}$ was estimated to be $> 85\%$ of the total uranium in all sediment samples using sediment extractions and x-ray absorption near-edge spectroscopy, which is consistent with model predictions.

The microbial community composition in sediment samples was characterized using PLFA, quantitative polymerase chain reaction (Q-PCR), and clone libraries (Michalsen et al. 2007). Measured PLFA biomass was not statistically different ($p = 0.01$) from simulated

biomass (Figure 7). Predictions that sulfate reducers and syntrophs would grow were confirmed by increased concentrations of several diagnostic PLFA groups compared to unstimulated sediment and included branched monounsaturates and mid-chain branched saturates, which are general indicators of sulfate reducing bacteria (Boon et al. 1997; Edlund et al. 1985) and dimethylacetals, indicators of Clostridia and some gram-negative bacteria (Mikell et al. 1986; Moore and Moore, 1998). Model predictions for the growth of denitrifiers was confirmed by the detection of dissimilatory nitrite reductase genes, *nirS* and *nirK*, and Q-PCR targets for iron and sulfate reducing bacteria (δ -proteobacteria), known iron reducing bacteria (*Geobacteraceae*), and methanogens. However, when the Q-PCR targets are expressed as a function of 16S Eubacterial rRNA, the microbial community consisted primarily of denitrifiers and iron and sulfate reducers (Figure 7). Although the model predicted that denitrifiers should make up only about 14 % of the microbial community at the time samples were collected (0.25 mol/kg ethanol reacted), Q-PCR suggested that denitrifiers made up almost 80 % of the community. Model predictions and Q-PCR results both indicated that iron- and sulfate-reducing bacteria should represent ~ 15-25 % of the community but Q-PCR results for methanogens (<0.01 %) were much smaller than predicted (note however that substantial methane production was observed during the experiments). No Q-PCR targets are available for the other major predicted groups, syntrophs and manganese reducers. *Geobacteraceae* were detected by Q-PCR at very low levels (< 0.01 %), which is also much smaller than the 15-25 % predicted for iron reducers by the model. Of course, direct comparisons of Q-PCR results and model predictions are problematic and it is possible that Q-PCR data reported here could vary by two orders of magnitude or more due to variability in the copy number of genes, the presence of DNA in decomposing cells, variability in extraction efficiencies, and other factors.

Information on community composition was also obtained from clone libraries from three sediment samples (Michalsen et al. 2007). Clone libraries developed from the sample collected nearest the column inlet were dominated by δ -proteobacteria consistent with model predictions for substantial growth of sulfate reducers, iron reducers, and syntrophs. Clone libraries from samples collected further from the model inlet, after soluble electron acceptors were largely depleted, were dominated by candidate division OP11, an uncultured group of Bacteria often found in anaerobic environments for which no physiological information is available, suggesting a possible role for OP11 in syntrophic growth. δ -proteobacteria clone sequences grouped into five families including *Geobacteraceae*, *Syntrophaceae*, *Desulfobulbaceae*, *Desulfobacteraceae*, and *Desulfovibrionaceae*.

FRC Area 1

Batch Simulations. For FRC Area 1, which has very high initial nitrate concentration (Table 2), ethanol addition was predicted to result in the growth of nine microbial groups in the batch simulations (Figure 8): ‘denitrifiers’ (NO_3^-/N_2)(Ethanol/ CO_2); ‘iron reducers’ ($\text{Fe}^{3+}/\text{Fe}^{2+}$)(Acetate/ CO_2); ‘methanogens’(CO_2/CH_4)(Acetate/ CO_2) and (CO_2/CH_4)(H_2/H^+); ‘manganese reducers’ ($\text{MnO}_4^-/\text{Mn}^{2+}$)(Acetate/ CO_2); ‘syntrophs’ (H^+/H_2)(Ethanol/Acetate); ‘sulfate reducers’ ($\text{SO}_4^{2-}/\text{HS}^-$)(Ethanol/Acetate); ‘aerobes’ ($\text{O}_2/\text{H}_2\text{O}$)(H_2/H^+); ‘uranium reducers’ ($\text{UO}_2^{2+}/\text{U}^{4+}$)(Acetate/ CO_2); and ‘technetium reducers’ ($\text{TcO}_4^-/\text{TcO}^{2+}$)(Acetate/ CO_2). However, growth of denitrifiers dominated the predicted community composition representing ~ 100 % of the total biomass for the first 50 mmol/kg of reacted ethanol. Growth of other groups was not energetically favorable until essentially all nitrate was consumed, after which ethanol became available to support the growth of other groups especially methanogens, iron reducers, and

manganese reducers, which grow on acetate produced by syntrophs. Growth of all other groups contributed < 1 % to the total biomass over the entire reaction path.

Growth of denitrifiers resulted in complete consumption of nitrate and the production of N_2 and CO_2 (which in water reacts to form HCO_3^-) (Figure 8). It is interesting to note that complete reduction of the very high initial nitrate concentration results in a predicted aqueous N_2 concentration of 50 mM, (not shown on figure), which exceeds N_2 's aqueous solubility ($\sim 700 \mu M$) predicting the evolution of substantial quantities of N_2 gas, which has been observed in laboratory experiments with FRC sediments (e.g., Istok et al. 2007). Subsequent growth of iron, manganese, uranium, sulfate, and technetium reducers resulted in the dissolution of goethite and pyrolusite, the precipitation of magnetite, rhodocrosite, pyrite, siderite ($Fe^{(II)}CO_3$), uraninite, and technetium sulfide, and the production of Mn^{2+} and Fe^{2+} . Acetate and H_2 eventually accumulated to a maximum concentration of ~ 10 nM because at the end of the reaction path, growth of microbial groups that utilize acetate and H_2 as electron donors becomes unfavorable due to the extremely low concentration of their electron acceptors. Microbial production of CO_2 and H^+ consumption resulted in an increase in pH from 3.5 to 8.0 and the precipitation of gibbsite [$Al(OH)_3$], calcite [$CaCO_3$], magnesite [$MgCO_3$], and siderite [$Fe^{(II)}CO_3$]. Interestingly, the formation of pyrite, siderite, magnesite, and magnetite maintained low aqueous Fe^{2+} and HS^- concentrations even during the growth of iron and sulfate reducers.

Comparison to experimental data. A series of single-well, push-pull tests were conducted in Area 1 wells FW028 and FW034 using methods described in Istok et al. (2004). Injected test solutions consisted of Area 1 groundwater (Table 2) amended with 300 mM ethanol and 1.25 mM Br^- as a conservative tracer; an adjacent test was conducted in well FW016 without added ethanol to serve as a control. Groundwater samples were collected periodically from all wells for

4-6 weeks and sediment cores were collected 5-7 m below land surface next to the wells after 1 week. DNA was extracted from core samples and analyzed by 16SrRNA, cloning, and sequencing as described by Spain et al. (2007). Geochemical data showed the complete consumption of oxygen, nitrate, and sulfate the production of Fe^{2+} and Mn^{2+} as predicted (Istok et al., 2004). Microbial analyses of sediment cores collected from near the injection wells at the end of the experiments showed that biostimulated cores are enriched in members of the classes β - and γ -proteobacteria with dominant clones related to known denitrifying bacteria. Together, these two classes make up 80-90% of the biostimulated clone libraries. Although the model predicted low levels of sulfate/metal reducing bacteria, the δ -proteobacteria, a group synonymous with metal/sulfate reduction made up 5-10% of the clones in one of the cores, indicating that in this sample nitrate had become depleted. Phospholipid fatty acids (PLFAs) analysis confirmed the results derived from the clone libraries.

Flush Simulations. ‘Flush’ simulations for the same initial geochemical system showed very different results than the ‘batch’ simulations (Figure 9). The continuing addition of unreacted porewater containing a very high nitrate concentration and the continued removal of dissolved N_2 as the reacted porewater was flushed from the system resulted in a ‘thermodynamic niche’ in which essentially only denitrifiers could obtain energy for growth and the growth of a single group (NO_3^-/N_2)(Ethanol/ CO_2) accounted for essentially ~ 100 % of all biomass production throughout the entire reaction path. Interestingly, aerobes and sulfate reducers did not grow to any extent despite the continued addition of oxygen and sulfate with each flush of unreacted porewater; the energy yield from growth of these groups was too small for them to compete with denitrifiers for ethanol when nitrate concentrations are this large.

Gibbsite and, to a lesser extent, alunite $[\text{KAl}_3(\text{SO}_4)_2(\text{OH})_6]$ were the only minerals to precipitate. Pyrolusite slowly dissolved as some aqueous $\text{Mn}^{(\text{IV})}$ species were flushed from the system. Significantly, the pe of the system remained positive throughout the simulation and no uraninite or Tc_2S_7 formed.

Comparison to experimental data. Flush simulations were compared to data from a second long-term column experiment conducted at the FRC. This column was 25 cm wide x 100 cm tall by 200 cm long, packed with ~ 720 kg uncontaminated site sediment and continuously perfused with site groundwater. Ethanol was injected daily to stimulate microbial growth and porewater samples were routinely collected from ports along the column length. After the last sampling event, eight sediment samples were collected for microbial community and geochemical characterization. Detailed experimental procedures and complete geochemical and microbiological results are summarized in Michalsen et al. 200X.

Similar to the simulations, the high nitrate concentration in influent groundwater dominated the response of the column to long-term ethanol additions. Nitrate concentrations exceeded 80 mM even after almost 100 mM ethanol had been consumed, sulfate concentrations did not decrease, and Fe^{2+} , Mn^{2+} , CH_4 were never detected during the experiment. Aqueous uranium concentrations decreased somewhat during the experiment, which Michalsen et al., attributed to sorption. Analyses of sediment samples by sequential chemical extraction and x-ray techniques indicated that sediment associated uranium was $\text{U}^{(\text{VI})}$. Pertecnetate concentrations also remained close to inlet values.

The microbial community composition in sediment samples was characterized using PLFA and Q-PCR (Michalsen et al. 200X). Measured PLFA biomass was ~ 1 order of magnitude smaller than predicted biomass (Figure 10). Predictions that sulfate reducers and

syntrophs would not grow under the conditions of this experiment were confirmed by no measured increase in branched monounsaturates and mid-chain branched saturates PLFAs (Boon et al. 1997; Edlund et al. 1985). Model predictions for the growth of denitrifiers were confirmed by the detection of dissimilatory nitrite reductase genes, *nirS* and *nirK*, which represented a large proportion of the total gene targets. Q-PCR targets for iron reducing bacteria (including *Geobacteraceae*) and sulfate-reducing bacteria were not detected.

Old Rifle

Batch simulations. The results of the ‘batch’ simulations predict that acetate addition would result in the growth of 13 of the 28 microbial groups in the database including: ‘aerobes’ ($\text{O}_2/\text{H}_2\text{O}$)(H_2/H^+) and ($\text{O}_2/\text{H}_2\text{O}$)(CH_4/CO_2); ‘manganese reducers’ ($\text{MnO}_4^-/\text{Mn}^{2+}$)(Acetate/ CO_2) and ($\text{MnO}_4^-/\text{Mn}^{2+}$)(H_2/H^+); ‘denitrifiers’ (NO_3^-/N_2)(Acetate/ CO_2) and (NO_3^-/N_2)(H_2/H^+); ‘iron reducers’ ($\text{Fe}^{3+}/\text{Fe}^{2+}$)(H_2/H^+); ‘sulfate reducers’ ($\text{SO}_4^{2-}/\text{HS}^-$)(Acetate/ CO_2); ‘syntrophs’ (H^+/H_2)(Ethanol/Acetate); ‘methanogens’ (H_2/H^+)(CO_2/CH_4) and (CO_2/CH_4)(Acetate/ CO_2); and ‘uranium reducers’ ($\text{UO}_2^{2+}/\text{U}^{4+}$)(Acetate/ CO_2) (Figure 11). The other groups in Table 1 did not appear because growth of these groups was not energetically favorable under these conditions (also, growth of technetium reducers was not predicted because no initial Tc was present). Most predicted biomass increase was due to the growth of iron reducers, sulfate reducers, and methanogens, with the proportion of methanogens increasing as sulfate, $\text{Mn}^{(\text{IV})}$, and $\text{Fe}^{(\text{III})}$ were gradually depleted. The predicted community composition consisted primarily (> 50 %) of iron reducers and sulfate reducers until 50 mmol/kg of acetate was reacted and decreased to ~ 27 % by the end of the reaction path. As in the batch simulations for the FRC, growth of methanogens dominated community composition once supplies of the more energetically favorable electron

acceptors were consumed and constituted ~ 60 % of the total biomass by the end of the reaction path.

Growth of aerobes, denitrifiers, and manganese reducers resulted in the consumption of available oxygen and nitrate, the dissolution of pyrolusite, and the precipitation of rhodocrosite after the first ~ 2 mmol/kg of acetate were reacted (Figure 11). Growth of iron reducers resulted in the dissolution of goethite and the precipitation of magnetite after 10 mmol/kg acetate were reacted. Calcite, magnesite, and siderite precipitated due to microbial production of CO₂ by several groups and Fe²⁺. Growth of uranium reducers resulted in the precipitation of U^(IV) as uraninite. The initial high quantity of sulfate was not completely consumed until ~ 85 mmol/kg acetate was reacted. Later in the reaction path methanogens and syntrophs grew but concentrations of methane, acetate, and hydrogen remained very small (<~0.1 nM). Microbial manganese and iron reduction decreased pe to ~ -5, which resulted in the predicted abiotic reduction of V^(V) to V^(IV).

Flush simulations. Flush simulations showed very different predicted patterns of microbial growth and community composition (Figure 12). Because of the continued addition of high amounts of sulfate with each flush of unreacted porewater, growth of sulfate reducers dominated throughout the reaction path, with much smaller predicted proportions of iron reducers, manganese reducers, and syntrophs compared to batch simulations (Figure 12 vs Figure 11). In particular, growth of methanogens was completely inhibited during flush simulations although growth of methanogens constituted ~ 65% of the total biomass by the end of the reaction path in batch simulations. Growth of manganese- and iron-reducers resulted in the dissolution of pyrolusite and goethite and the precipitation of rhodocrosite and magnetite. Microbial CO₂ production and increased pH resulted in the precipitation of calcite (but not magnesite predicted

in batch simulations) and growth of sulfate reducers resulted in the precipitation of pyrite (but not siderite predicted in batch simulations). Even though sulfate reduction was the dominant microbial growth process, sulfate was never completely consumed and reached an equilibrium concentration of ~ 3.6 mM. The high level of available sulfate and the continued removal of Fe^{2+} by pyrite precipitation and flushing of reacted porewater makes sulfate reduction the most energetically favorable growth process throughout the reaction path, and the accumulation of H_2 and methane predicted in batch simulations was not predicted in flush simulations. Growth of uranium reducers resulted in the precipitation of uraninite. Once, p_e fell below ~ -3.2 , $\text{V}^{(\text{V})}$ was abiotically reduced to $\text{V}^{(\text{IV})}$.

Comparison to experimental data. Natural gradient field experiments have been conducted at Old Rifle for several years to study the affects of acetate addition on microbial activity and the geochemistry of U and V (Anderson et al., 2003; Ortiz-Bernad et al., 2004, Vrionis et al 2005). In the first field experiment (Anderson et al., 2003), acetate was injected into the aquifer for three months with a targeted in situ acetate concentration of ~ 3 mM. Groundwater samples were collected from 15 monitoring wells located 3 - 15 m downgradient from the injection wells. Background samples were collected from 3 wells located ~ 3 m upgradient of the injection wells. In addition to geochemical analyses, groundwater samples from selected wells (including M-7) were used to develop clone libraries of the unattached microbial community; microbial samplers were also deployed in this well and analyzed for lipids as a way to monitor changes in community composition during the experiment. Experimental data were plotted on computed reaction paths using the cumulative quantity of acetate consumed at the time of each sampling event as the independent variable. The latter was calculated using measured concentration and volume of injected acetate solutions, groundwater travel times from the injection wells to M-7

determined from bromide tracer tests, and measured acetate concentrations at M-7 during the experiment.

Simulations were in general agreement with experimental data with some important exceptions. A variety of considerations such as sampling frequency, analytical detection limits, and analytical protocols, combined with the uncertainty of certain model input parameters made a rigorous comparison of simulations and field measurements problematic. Simulated and measured pHs matched closely (Figure 13). Simulated pe values were generally lower than those computed from field measurements with a platinum electrode. Nitrate was predicted to be completely consumed and was not detected in groundwater samples from M-7. Sulfate concentrations were predicted to decrease and then reach a plateau due to the continual influx of sulfate from upgradient and these were in close agreement with measured values. However, in some wells and in column experiments (N'Geussan 2006), sulfate values approach zero, suggesting that sulfate and acetate fluxes varied, at least in part, due to heterogeneity in the groundwater flow system, which influenced delivery of soluble electron acceptors and acetate to specific monitoring wells. $U^{(VI)}$ concentrations were predicted to decrease due to growth of uranium reducers and measured $U^{(VI)}$ concentrations did decrease to very low levels ($\sim 0.2 \mu M$) but were larger than predicted. Decreasing pe resulting from the growth of iron reducers and sulfate reducers was predicted to cause the reduction of $V^{(V)}$ and a decrease in aqueous $V^{(V)}$ concentrations were observed during the experiment. Model simulations predicted an increase in Fe^{2+} due to the growth of iron reducers as observed during the experiment, however measured Fe^{2+} values were generally larger than predicted. This observation is particularly significant since sorption of Fe^{2+} (which was not considered in model simulations) would be expected to decrease measured aqueous Fe^{2+} values (Yabusaki et al. 2007). One possible explanation for this

discrepancy may be the uncertainty in initial quantities of bioavailable $\text{Fe}^{(\text{III})}$ used in model simulations although no additional experimental information are available to investigate this conjecture. No field data were collected for Mn^{2+} .

Although no sediment data were collected to compare to model mineral predictions, it is interesting to note that the model predicted the complete dissolution of goethite during the experiment after 20-25 mmol/kg of acetate was reacted. Depletion of bioavailable $\text{Fe}^{(\text{III})}$ was proposed by Anderson et al. as a potential explanation for measured shifts in microbial community composition, discussed below. Dissolution of pyrolusite and precipitation of rhodocrosite, magnetite, calcite, and uraninite were also predicted.

Model simulations predicted an increase in total biomass of $\sim 1.5 \times 10^8$ cells/gram consisting primarily of sulfate reducers, iron reducers, manganese reducers, and denitrifiers with an increasing percentage of sulfate reducers as more acetate was reacted (Figure 14). PLFA was extracted from biomass retained on microbial samplers deployed and periodically removed from several of the monitoring wells (Anderson et al. 2003). From these data the maximum viable PLFA biomass was estimated at $10^7 - 10^8$ cells/gram and PLFA diagnostic of known iron reducers (*Geobacteraceae*) represented $\sim 30 - 40\%$ of the total biomass, which is consistent with model predictions.

Clone libraries developed from groundwater samples collected from M-7 provided a more complete description of the (unattached) microbial community composition during the experiment (Figure 13). The clone libraries confirmed the predicted growth of denitrifiers, sulfate reducers, and iron reducers during the experiment. Simulations also predicted a decreasing percentage of iron reducers and manganese reducers as supplies of $\text{Fe}^{(\text{III})}$ and $\text{Mn}^{(\text{IV})}$ were depleted and high concentrations of sulfate were continuously added to the system as

background groundwater entered the treatment zone. In the clone libraries, iron reducing organisms, which constituted up to 85 % of the total community composition early in the experiment, decreased to less than 10 % at the end of the reaction path. It is noteworthy that subsequent field experiments have looked more closely at the early phase Fe-reduction. These results indicate that the unattached community is dominated by Geobacters, in some cases as much as 95%, commonly a single species.

DISCUSSION

The modeling approach presented here was developed to predict microbial growth and changes in community composition and system geochemistry that occur when a growth-limiting-substrate is added to a subsurface environment. For this paper, the number and kind of microbial groups were selected to capture the major features of system dynamics observed during laboratory and field experiments that investigated the reductive precipitation or ‘bioimmobilization’ of U and Tc. Of course alternate microbial groups could be specified by selecting additional or different microbial groups as needed for other applications. Growth equations can be derived using methods in Rittmann and McCarty (2001) or Heijnen (1991), or directly from system-specific growth data. The approach developed by Heijnen and coworkers is particularly powerful because it has the potential to greatly reduce the number of adjustable model parameters. For example, all simulations presented here were performed with 28 microbial groups whose growth equations, biomass yields, and standard-state free energy of reaction were derived using a combination of methods from Rittmann and McCarty (2001) and Heijnen et al. 1992. In general, each growth equation required the specification of a single parameter (one per group) for a total of 28 microbial parameters. Although this is substantially smaller than the number of parameters that would be required for a kinetic model of such a

complex microbial community, which would require several hundred kinetic parameters, it is possible that using Heijnen's approach the number of parameters required to derive *all* the growth equations in Table 1 could be reduced to a total of *three* (i.e. the D_s^{01}/r_{AX} values for ethanol, acetate, and H_2). Moreover, Heijnen and van Dijken (1992) tabulated D_s^{01}/r_{AX} for a large number of common growth substrates and presented correlations (with carbon chain length and degree of reduction) that can be used to estimate a value of D_s^{01}/r_{AX} for substrates not tabulated. Thus, it should be possible to derive growth equations for many more microbial groups than those presented here and, in time, a comprehensive thermodynamic data base for microbial growth containing many hundred such equations could be compiled, similar to existing data bases compiled for geochemical reactions. The relatively small number of parameters required should facilitate wide-spread use of the model and a more direct comparison between data and model simulations across a variety of investigators and experimental settings.

Once the growth equations have been derived and appended to an appropriate thermodynamic database and the initial geochemical composition is specified, the effects of prescribed electron donor addition on the system biogeochemistry are predicted by simultaneously solving the coupled system of microbial growth equations and geochemical reactions in the database. At each point along the reaction path, only those reactions that are thermodynamically favorable will proceed. By combining the thermodynamics of microbial growth and geochemical reactions, the modeling approach presented here directly and naturally couples these processes. The geochemical environment is described by a thermodynamic database that describes mineral precipitation/dissolution and many other reactions. Simulations were performed with the program REACT and the LLNL database, but many other programs,

including those in the public domain, and many other thermodynamic databases have been compiled for use in specific geochemical environments (Bethke, 1996).

Clearly, the modeling approach presented here is based on a number of simplifying assumptions about the physiological responses of microorganisms to changing environmental conditions and the kinetics of growth and geochemical reactions that may or may not be valid in any particular experimental setting. For example, organisms in each microbial group are assumed to catalyze a single oxidation-reduction reaction with a fixed growth stoichiometry and biomass yield that are independent of substrate concentration, exposure time, predation, toxicity, or any other microbial or geochemical variable. The kinetics of microbial growth are ignored entirely as predicted growth and community composition are based solely on the quantity of substrate reacted, regardless of the time required for this to occur. However, it should be noted that it is possible to connect model predictions to experimental data by converting substrate concentrations measured as a function of time to quantity of substrate reacted and plotting experimental data using reacted substrate as the independent variable, as was done to compare model predictions to the FRC and Old Rifle experiments. It may be possible that during periods of rapid growth that occur following the addition of a growth-limiting substrate to an oligotrophic environment, the kinetics of microbial growth are generally faster than that of many geochemical reactions (e.g. the kinetics of mineral dissolution and precipitation reactions) and that the latter may exert more control on the validity of equilibrium reaction path calculations than the former. However, the validity of all of these assumptions waits additional model testing.

Despite the large number of simplifying assumptions used in model development, it is surprising and encouraging that the simulations were in general agreement with experimental

data from batch and column laboratory experiments and field experiments conducted at the FRC and Old Rifle (the only sites where bioimmobilization of U and Tc has been studied in any detail). In particular, it is remarkable that a model based on the same small set of parameters could be successfully applied to such disparate geochemical environments (e.g. pH from 3.3 to 7.3; NO_3^- from 0.1 to 100 mM, SO_4^{2-} from 0.4 to 6.4 mM).

Nevertheless, strict verification of model predictions will be difficult as various constraints limit our ability to perform the necessary measurements. Groundwater geochemical measurements alone are insufficient to verify model predictions because of the important role that mineral dissolution and precipitation have on the energetics of microbial growth. Many analytical protocols are subject to uncertainties in interpretation and some important minerals (uraninite and particularly technetium sulfide) may be present at such low concentrations, even in contaminated environments, that they can not be accurately quantified by any available technique. Perhaps the largest geochemical uncertainty in model simulations presented here were the initial mineral forms and quantities of bioavailable $\text{Fe}^{(\text{III})}$ and $\text{Mn}^{(\text{IV})}$. Clearly microbial reduction of mineral oxides is complex and undoubtedly kinetically controlled, with quantities of reducible $\text{Fe}^{(\text{III})}$ and $\text{Mn}^{(\text{IV})}$ changing with time in response to microbial growth and many other environmental variables. Interestingly, microbial dissolution of these minerals can lead to the formation of carbonate minerals that exert control on HCO_3^- concentration and thus on the growth of several other microbial groups (e.g., methanogens).

Model simulations presented here also ignored the sorption of aqueous species to mineral surfaces. While it is possible to include sorption of aqueous species to mineral surfaces in the thermodynamic database used in REACT, we ignored sorption in the

simulations presented here for two reasons: (1) required sediment parameters (e.g. chemical composition and reactive surface area of sorption sites) were not measured in any of the experiments, and (2) sensitivity analyses (not shown) suggest that sorption will have relatively little effect on microbial growth, especially if $\text{Fe}^{(\text{II})}$ -bearing mineral phases precipitate (i.e, the free energy yields for growth of e.g. iron reducers is relatively insensitive to aqueous Fe^{2+} concentrations in the range observed in these experiments). However, we recognize that sorption of Fe^{2+} was identified as an important factor in a kinetic, reactive transport model developed for the Old Rifle site (Yabusaki et al., 2007).

Verifying model predictions for microbial growth and community composition is likewise difficult for several reasons. While, robust and reliable methods for detecting total viable biomass are available (e.g., PLFA), and Q-PCR and clone libraries can detect and quantify specific gene targets or phylogenetic groups, there is generally no direct correspondence between these biomarkers and the microbial groups derived from thermodynamic considerations. It is recognized that many microbial groups that could be detected by lipid or nucleic acid biomarkers may share certain metabolic capabilities or shift from one physiological state to the next as environmental conditions change, confounding data interpretation. For example, the PLFA profile of an environmental microbial community is dictated by the proportions of different organisms present and their metabolic state, though this information can not usually be “decoded” to a list of specific organisms or their abundances (Federle et al., 1983). However when complimentary nucleic acid information is obtained, such as clone libraries, the PLFA profiles can be parsed according to the specific nucleic acid results (as was done for Old Rifle by Anderson et al., 2003). The combination of lipid biomarker analysis (quantitative but not specific) and nucleic acid-based

analyses (specific but not quantitative) greatly expands the specificity and scope of community compositional determinations (Leung et al., 1999).

It would be desirable to have biomarkers for iron- and manganese-reducers as growth of these groups seems to be thermodynamically favorable at the FRC and Old Rifle sites, they are important in uranium and technetium reduction, and because, in some cases, they are predicted to represent a large proportion of the total community. Perhaps the most straightforward approach to testing model predictions would involve direct quantification of the functional genes responsible for each group's metabolic function. For well characterized pathways such as nitrate reduction, quantitative assays such as real-time PCR enumeration of nitrite reductase genes (*nirS* and *nirK*) have been developed and serve as an appropriate index of nitrate reducers (Braker et al., 1998). Conversely for metabolic functions such as iron reduction, choosing an adequate functional indicator gene among the myriad of outer membrane cytochromes believed to be involved in iron and manganese reduction has been more difficult. While qPCR protocols directed at quantification of citrate synthase (Chin et al., 2004) and outer membrane cytochrome *omcB* (Holmes et al., 2005) mRNA transcripts of *Geobacteraceae* have been used as an indicator of iron reduction activity, a general genetic biomarker for iron reduction is not currently available. Fundamental research to further elucidate metabolic functions will certainly aid in the characterization of key metabolic processes, however, nucleic acid microarray technologies, particularly functional gene arrays (FGAs), will likely have the most immediate impact on our understanding of microbial diversity, abundance, and activity in the environment. The greatest advantage of an FGA platform is the ability for highly multiplexed detection. Therefore, an FGA could not only be used to evaluate the on-going metabolic activities (denitrification or iron reduction) but also more adequately address the

breadth of organisms capable of a particular metabolic function. Furthermore, the incorporation of multiple genes involved in a particular metabolic function provides a level of redundancy to conclusively characterize the dominant metabolic functions of a diverse microbial community. Nevertheless, model predictions were in general agreement with the combination of lipid and nucleic acid measurements performed in the experiments, and provide encouragement that, with the further development of molecular biological tools, more rigorous model testing will be possible. Of course all measurements in complex natural systems are subject to uncertainties caused by spatial and temporal heterogeneity and by scaling measurements across a variety of spatial and temporal scales. (It might be noted that there is an interesting aspect of the proposed modeling approach related to scaling. The only required system-specific model inputs are those that describe the geochemical composition of the system, which by definition scales exactly. Thus the same modeling approach can be applied to systems with very spatial scales providing a theoretically rigorous way to compare experimental results from small- to large-scale laboratory and field experiments.)

Despite all the assumptions used in its development, we believe the modeling approach presented here will be a useful tool for investigating several aspects of the complex coupling between microbial growth and geochemical reactions that occurs when substrates are added to a natural environment to stimulate microbial growth. Differences between the ‘batch’ and ‘flush’ simulations are particularly interesting because they represent the two main experimental systems that have been used to study bioimmobilization of radionuclides (as well as many other systems of interest in environmental biotechnology). The ‘batch’ simulations model a closed laboratory microcosm bottle, with fixed volume and zero mass transfer in or out of the bottle (except for the substrate additions). As the simulations show, when electron donor is added to

such a system, the availability of aqueous and solid phase electron acceptors continuously decrease. The general sequence of microbial processes follows the usual progression of TEAPS except that these are ordered by the system specific geochemical environment, which we have referred to as a 'thermodynamic niche'. In natural systems, the specific TEAP is thought to be largely controlled by the thermodynamic threshold levels of microbial intermediates such as acetate and H_2 (Lovley and Goodwin 1988); microorganisms will grow and maintain the concentration of these intermediates at a minimum level, determined by the minimum energy yield needed for their growth. As the minimum energy yield is thought to be equivalent across bacterial groups, bacteria carrying out respiratory processes yielding more energy can draw the H_2 or acetate concentrations to lower levels and will outcompete those carrying out lower energy yielding processes. Our modeling approach incorporates this concept, allowing H_2 and acetate to be produced forcing competition between different microbial groups allowing the process yielding the most energy to dominate. It should be noted that the modeling approach presented here is a potentially useful tool for comparing the effects of alternate growth-limiting substrates on overall system behavior and should prove useful for experimental design and hypothesis testing. It will also be useful to explore the effects of other system variables on resulting growth and community composition in a more systematic way so that questions of community stability (e.g. to changing pH) can be addressed.

Similarly, relative abundances of oxygen, nitrate, sulfate, $Fe^{(III)}$, and $Mn^{(IV)}$ can affect the ordering of the major TEAPs. For example, when nitrate concentrations are very high as at the FRC and other contaminated sites, denitrification can be more energetically favorable than aerobic respiration. The simulations clearly show that more than one TEAP can be operational simultaneously and that diagnostic metabolic products can accumulate (e.g., N_2 or CH_4) if no

other group can utilize them as growth substrates, and they do not participate in geochemical reactions. Alternatively, the concentration of metabolic products that are produced in large amounts (e.g., Fe^{2+} or HS^-) will decrease if they participate in abiotic geochemical reactions (e.g. mineral precipitation) that remove them from solution.

For the same initial geochemistry and quantities of reacted substrate flush simulations predicted very different total biomass and microbial community composition than batch simulations. In the flush simulations, which were used to describe laboratory column experiments and certain natural gradient field tests, the addition of soluble electron acceptors (e.g. O_2 , NO_3^- , and SO_4^{2-}) with each increment of added substrate and the removal of soluble metabolic products (e.g. N_2 , Fe^{2+} , HS^-) profoundly changed the thermodynamic niche resulting in substantial shifts in community composition and geochemical environment compared to batch simulations. As the biomass yields for some groups (esp. denitrifiers) are generally larger than yields for manganese reducers and iron reducers (Table 1), the total biomass produced for each increment of electron donor reacted was much larger for flush simulations than for batch simulations. Also, the continuous influx of soluble electron acceptors means that the growth of microbial groups that utilize them (e.g. aerobes, denitrifiers, and sulfate reducers) dominate community composition throughout the reaction path during flush simulations compared to their generally decreasing proportion of community composition during batch simulations.

A number of theories have been developed in macrocommunity ecology to describe the relationship between community composition (species diversity) and ecosystem function (Lawton, 1994). Wardle and Giller (1996) suggested that the broad genetic diversity and metabolic functionality and potential for rapid growth of subsurface microorganisms provide an excellent opportunity to test certain aspects of ecological theory. However, only a few studies

have addressed this relationship for microbial communities in either natural or engineered ecosystems (Mikola and Setälä, 1998; Griffiths, et al., 2000; Müller et al., 2002). Although high levels of genetic diversity have been empirically correlated with high stability in community function (e.g., Griffiths et al., 2000), the validity of this hypothesis as a general ecological concept is controversial (Grime, 1997). Moreover, the level or degree of diversity required to impart stability to a community is unknown (Wardle and Giller, 1996). The goal of U and Tc bioimmobilization is to stimulate microbial activity to result in the precipitation of $U^{(IV)}$ as uraninite and $Tc^{(IV)}$ as Tc_2S_7 (and related mineral phases). The simulations presented here have shown the cooperative metabolism of many microbial groups is required (1) to create a thermodynamic niche that allows uranium- and technetium-reducers to grow and (2) to create a geochemical environment that favors the stability of $U^{(IV)}$ and $Tc^{(IV)}$ mineral phases. Because U and Tc are typically present at much smaller concentrations (pM to uM) than competing electron acceptors (mM), predicted community composition in both batch and flush simulations is dominated by the growth of those groups that catalyze the reduction of NO_3^- , SO_4^{2-} , $Fe^{(III)}$, $Mn^{(IV)}$, methanogens, and syntrophs. In all cases growth of uranium reducers and technetium reducers contributed negligible biomass to overall community composition.

The simulations for FRC and Old Rifle provide important insights into the coupling between microbial growth and geochemical reactions that occur when substrates are added to the subsurface to create conditions that favor reductive precipitation of U and Tc. However, the modeling approach presented here is more general and can be easily modified to address other environmental and biotechnological problems and processes. Thus, the thermodynamic data base (i.e. Table 2) can be easily extended to incorporate additional microbial groups and growth substrates, inorganic or organic contaminants, etc. These could also include, for example,

microbial groups that obtain energy for growth by oxidizing reduced species such as HS^- , Fe^{2+} , etc. and these combined with groups that reduce sulfate, $\text{Fe}^{(\text{III})}$, etc. could be used to study mineral cycling the environment. Perhaps the most important feature of the model is that it makes quantitative predictions about the effects of microbial growth on community composition and system geochemistry. Recent advances in molecular biology and geochemistry will soon make it possible to make measurements specifically designed to test model predictions. The promise of an experimentally verifiable modeling approach that is based on thermodynamic principles and only a few adjustable parameters is exciting and offers a fundamentally new way to explore issues of microbial community ecology. In this regard, the concept of a ‘thermodynamic niche’ seems to provide a particularly compelling way to look at microbial community structure and its change through space and time. The ‘thermodynamic niche’ is in some ways an extension of the useful TEAP concept but recognizes that there is no simple defined order of microbial growth processes that will occur, especially at sites with very large concentrations of soluble electron acceptors such as the FRC, Old Rifle, and other contaminated sites where denitrification and sulfate reduction can dominate growth throughout the reaction path.

An additional logical step would be to couple the thermodynamic approach for predicted microbial growth with a reactive flow and transport model to describe the site-scale effects of substrate addition on microbial growth and geochemistry and would allow a more complete description of the formation and progress of reaction fronts as they are swept through the subsurface by well-known process of advection and dispersion. This approach could potentially provide additional insight into all of these processes and would represent an important advance in our ability to describe conditions in a dynamic subsurface environment.

LITERATURE CITED

- Abdelouas, A. M. Fattahi, B. Grambow, L. Vichot, and E. Gautier. 2002. Precipitation of technetium by subsurface sulfate-reducing bacteria. *Radiochimica Acta*. 90:773-777.
- Anderson, T.T., H.A. Vrionis, I. Ortiz-Bernard, C.T. Resch, P.E. Long, R. Dayvault, K. Karp, S. Marutzky, D.R. Metzler, A. Peacock, D.C. White, M. Lowe, and D.R. Lovley. 2003. Stimulating the in situ activity *Geobacter* species to remove uranium from the groundwater of a uranium-contaminated aquifer. *Applied and Environmental Microbiology*, 69: 5884-5891.
- Baedecker, M.J. and W. Back. 1979. Hydrogeological processes and chemical reactions at a landfill. *Ground Water*, 17(5):479-437.
- Banwart, S.A. and S.F. Thornton. 2003. The geochemistry and hydrology of groundwater bioremediation by natural attenuation. In: *Bioremediation: a critical review*. I.M. Head, I. Singleton, and M. G. Milner (Eds.). Horizon Scientific Press. Wymondham. p. 93-138.
- Battley, E. H. 1987. *Energetics of microbial growth*. John Wiley & Sons, New York. 450 p.
- Benner, S. G., C. M. Hansel, B. W. Wielinga, T. M. Barber, and S. Fendorf. 2002. Reductive dissolution and biomineralization of iron hydroxide under dynamic flow conditions. *Environmental Science & Technology*, 36:1705-1711.
- Bethke, C.M. 1996. *Geochemical reaction modeling: Concepts and applications*. Oxford University Press, New York. 397 p.
- Beyenal, H., and Z. Lewandowski. 2001. Mass-transport dynamics, activity, and structure of sulfate-reducing biofilms. *Aiche Journal*, 47:1689-1697.

- Bjerg, P.L., K. Ruge, J.K. Pedersen, and T.H. Christensen. 1995. Distribution of redox-sensitive groundwater quality parameters downgradient of a landfill (Grindsted, Denmark). *Environmental Science & Technology*, 29:1387-1394.
- Boon, J. J. D. L., J. W.; Hoek, G. J.; Vosjan, J. H. 1977. Significance and Taxonomic Value of Iso and Anteiso Monoenoic Fatty Acids and Branched β -Hydroxy Acids in *Desulfovibrio desulfuricans*. *Journal of Bacteriology* 129:1183-1191.
- Braker, G., A. Fesefeldt, and K.-P. Witzel. 1998. Development of PCR Primer Systems for Amplification of Nitrite Reductase Genes (*nirK* and *nirS*) To Detect Denitrifying Bacteria in Environmental Samples. *Applied and Environmental Microbiology* 64:3769-3775.
- Brodie, E.L., T.Z. DeSantis, D.C. Joyner, S.M. Baek, J.T. Larsen, G.L. Andersen, T.C. Hazen, P.M. Richardson, D.J. Herman, T.K. Tokunaga, J.M. Wan, and M.K. Firestone. 2006. Application of high-density oligonucleotide microarray approach to study bacterial population dynamics during uranium reduction and reoxidation. *Applied Environmental Microbiology*, 72(9): 6288-6298.
- Bulger, P.R., A.E. Kehew, and R.A. Nelson. 1989. Dissimilatory nitrate reduction in a wastewater contaminated aquifer. *Ground Water*, 27(5):664-671.
- Burgos, W. D., R. A. Royer, Y. L. Fang, G. T. Yeh, A. S. Fisher, B. H. Jeon, and B. A. Dempsey. 2002. Theoretical and experimental considerations related to reaction-based modeling: A case study using iron(III) oxide bioreduction. *Geomicrobiology Journal*, 19:253-287.
- Chandler, D.P., S-M. Li, C.M. Spadoni, G.R. Drake. D.L. Balkwill, J.K. Fredrickson, and F.J. Brockman. 1997. A molecular comparison of culturable aerobic heterotrophic bacteria and

- 16S rRNA clones derived from a deep subsurface sediment. *FEMS Microbiol Ecology*, 23: 131.
- Chappelle, F.H. 2001. *Ground-water microbiology and geochemistry*. Wiley & Sons, New York.
- Chappelle, F.H. and D.R. Lovley. 1992. Competitive exclusion of sulfate reduction by Fe(III)-reducing bacteria: a mechanism for producing discrete zones of high-iron ground water. *Ground Water*, 30:29-36.
- Chappelle F. H., Haack S. K., Adriaens P., Henry M. A., and Bradley P. M. 1996. Comparison of Eh and H₂ measurements for delineating redox processes in a contaminated aquifer. *Environmental Science and Technology*, 30:3565-3569.
- Chappelle F. H., Mamahon P. B., Dubrovsky N. M., Fujii R. F., Oaksford E. T., and Vroblesky D. A. 1995. Deducing the distribution of terminal electron-accepting processes in hydrologically diverse groundwater systems. *Water Resources Research*, 31:359-371.
- Chin, K.-J., A. Esteve-Nunez, C. Leang, and D. R. Lovley. 2004. Direct Correlation between Rates of Anaerobic Respiration and Levels of mRNA for Key Respiratory Genes in *Geobacter sulfurreducens*. *Applied and Environmental Microbiology* 70:5183-5189.
- Coates, J. D., V. K. Bhupathiraju, L. A. Achenbach, M. J. McInerney, and D. R. Lovley. 2001. *Geobacter hydrogenophilus*, *Geobacter chappellei* and *Geobacter grbiciae*, three new, strictly anaerobic, dissimilatory Fe(III)-reducers. *International Journal of Systematic and Evolutionary Microbiology*, 51:581-588.
- Cord-Ruwisch, R., D. R. Lovley, and B. Schink. 1998. Growth of *Geobacter sulfurreducens* with acetate in syntrophic cooperation with hydrogen-oxidizing anaerobic partners. *Applied Environmental Microbiology*, 64:2232-2236.

- Coutts, D.A.P., E. Senior, and M.T.M. Balba. 1987. Multi-stage chemostat investigation of interspecies interactions in a hexanoate-catabolizing microbial association isolated from anoxic landfill. *J. Applied Bacteriology*, 62, p. 731-740.
- Cui, D. and T. E. Eriksen. 1996. Reduction of pertechnetate by ferrous iron in solution: influence of sorbed and precipitated Fe(II). *Environmental Science & Technology*, 30(7): 2259 – 2262.
- Delany, J.M. and S.R. Lundeen. 1989. The LLNL thermochemical database. Lawrence Livermore National Laboratory Report UCRL-21658.
- Drever, J. I., 1992. *The Geochemistry of Natural Waters*, Second edition, Prentice Hall, Englewood Cliffs, New Jersey.
- Edlund, A. N., P. D.; Roffey, R.; White, D. C. 1985. Extractable and lipopolysaccharide fatty acid and hydroxy acid profiles from *Desulfovibrio* species. *Journal of Lipid Research* 26:982-988.
- Federle, T. W., M. A. Hullar, R. J. Livingston, D. A. Meeter, and D. C. White. 1983. Spatial distribution of biochemical parameters indicating biomass and community composition of microbial assemblies in estuarine mud flat sediments. *Applied Environmental Microbiology*. 45:58-63.
- Fraterrigo, J.M., T.C. Balser, and M.G. Turner. 2005. Microbial community variation and its relationship with nitrogen mineralization in historically altered forests. *Ecology*: 87(3):570-579.
- Fredrickson, J. K., H. M. Kostandarithes, S. W. Li, A. E. Plymale, and M. J. Daly. 2000. Reduction of Fe(III), Cr(VI), U(VI), and Tc(VII) by *Deinococcus radiodurans* R1. *Applied Environmental Microbiology*, 66:2006-2011.

- Fredrickson, J. K., J. M. Zachara, D. W. Kennedy, C. X. Liu, M. C. Duff, D. B. Hunter, and A. Dohnalkova. 2002. Influence of Mn oxides on the reduction of uranium(VI) by the metal-reducing bacterium *Shewanella putrefaciens*. *Geochimica Et Cosmochimica Acta*, 66:3247-3262.
- Fredrickson, J. K., J. M. Zachara, D. W. Kennedy, H. L. Dong, T. C. Onstott, N. W. Hinman, and S. M. Li. 1998. Biogenic iron mineralization accompanying the dissimilatory reduction of hydrous ferric oxide by a groundwater bacterium. *Geochimica Et Cosmochimica Acta*, 62:3239-3257.
- Ghiorse, W.C. and Wilson, J.T. 1988. Microbial ecology of the terrestrial subsurface. *Advances in Applied Microbiology*, 33, p. 107-172.
- Ginn, T. R., E. M. Murphy, A. Chilakapati, and U. Seeboonruang. 2001. Stochastic-convective transport with nonlinear reaction and mixing: application to intermediate-scale experiments in aerobic biodegradation in saturated porous media. *Journal of Contaminant Hydrology*, 48:121-149.
- Grime, J.P. 1997. Biodiversity and ecosystem function: the debate deepens. *Science*, 277, 1260-1261.
- Heijnen, J.J. 1991. A new thermodynamically based correlation of chemotrophic biomass yields. *Antonie van Leeuwenhoek*, 60, 235-236.
- Heijnen, J.J. and J.P. van Dijken. 1992. In search of a thermodynamic description of biomass yields for the chemotrophic growth of microorganisms. *Biotechnology and Bioengineering*, 39, 833-858.
- Holmes, D. E., K. P. Nevin, R. A. O'Neil, J. E. Ward, L. A. Adams, T. L. Woodard, H. A. Vrionis, and D. R. Lovley. 2005. Potential for Quantifying Expression of the *Geobacteraceae*

- Citrate Synthase Gene To Assess the Activity of Geobacteraceae in the Subsurface and on Current-Harvesting Electrodes. *Applied and Environmental Microbiology* 71:6870-6877.
- Hubbel, S.P. 2001. The unified neutral theory of biodiversity and biogeography. Princeton University Press, Princeton, NJ.
- Istok, J.D., J.S. Senko, L. R. Krumholz, D. Watson, M.-A. Bogle, A. Peacock, Y-J. Chang, and D.C. White. 2004. In situ bio-reduction of technetium and uranium in a nitrate-contaminated aquifer. *Environmental Science Technology*, 38(2): 468 – 475.
- Istok, J.D., M.M. Park, A.D. Peacock, M. Oostrom and T.W. Wietsma. 2007. An Experimental Investigation of the Fate of Nitrogen Gas Produced During Denitrification. *Ground Water* 45(4): 461-467.
- Jain, D.K. S. Stroes-Gascoyne, M. Providenti, C. Tanner, and I. Cord. 1997. Characterization of microbial communities in deep groundwater from granitic rock. *Canadian Journal of Microbiology*, 43, p. 272-283.
- Jin, Q and C. M. Bethke. 2003. A new rate law describing microbial respiration. *Applied Environmental Microbiology*. 69(4): 2340–2348.
- Karthikeyan, S., G.M. Wolfaardt, D.R. Korber, and D.E. Caldwell. 1999. Functional and structural responses of a degradative microbial community to substrates with varying degrees of complexity in chemical structure. *Microbial Ecology*, 38, p. 215-224.
- Kieft, T.L., D.B. Ringelberg, and D.C. White. 1994. Changes in ester-linked phospholipid fatty acid profiles of subsurface bacteria during starvation and desiccation in a porous medium. *Applied Environment Microbiology*, 60: 3293-3299.
- Kostka, J. E., D. D. Dalton, H. Skelton, S. Dollhopf, and J. W. Stucki. 2002. Growth of iron(III)-reducing bacteria on clay minerals as the sole electron acceptor and comparison of growth

- yields on a variety of oxidized iron forms. *Applied and Environmental Microbiology* 68:6256-6262.
- Lawton, J.H. 1994. What do species do in ecosystems ? *Oikos*, 71, p. 367-374.
- Leung, K. T., Y.-J. Chang, Y.-D. Gan, A. Peacock, S. J. Macnaughton, J. R. Stephen, R. S. Burkhalter, C. A. Flemming and D. C. White. 1999. Detection of *Sphingomonas* spp. in soil by PCR and sphingolipid biomarker analysis. *J. Industrial Microbiology* 23:252-260.
- Liu, C., and J. M. Zachara. 2001. Uncertainties of Monod kinetic parameters nonlinearly estimated from batch experiments. *Environmental Science & Technology* 35:133-141.
- Lloyd, J. R., Sole, V. A., Van Praagh, C. V. G., Lovley, D. R. Direct and Fe(II)-Mediated Reduction of Technetium by Fe(III)-Reducing Bacteria *Applied Environmental Microbiology*, 66: 3743-3749.
- Lovley D. R. and S. Goodwin. 1988. Hydrogen concentrations as an indicator of the predominant terminal electron-accepting reactions in aquatic sediments. *Geochimica et Cosmochimica Acta* 52, 2993-3003.
- Lovley, D. R., E. J. P. Phillips, Y. A. Gorby, and E. R. Landa. 1991. Microbial reduction of uranium. *Nature (London)* 350: 413-416.
- Lovley, D.R. and F.H. Chapelle. 1995. Deep subsurface microbial processes. *Rev. Geophys.*, 33, p. 365-381.
- Lovley, D.R., F.H. Chapelle, and J.C. Woodward 1994. Use of dissolved H₂ concentrations to determine distribution of microbially catalyzed redox reactions in anoxic groundwater, *Environmental Science & Technology*, 28:1206-1210,
- Lovley, D.R., S.J. Giovannoni, D.C. White, J.E. Champine, E.J.P. Phillips, Y.A. Gorby, and S. Goodwin. 1993. *Geobacter metallireducens* gen. nov. sp. nov., a microorganism capable of

coupling the complete oxidation of organic compounds to the reduction of iron and other metals. *Arch. Microbiol.*, 159, p. 336-344.

MacArthur, R. and W. Wilson. 1967. *The theory of island biogeography*. Princeton University Press, Princeton, NJ.

Madigan, M.T., J.M. Martinko, and J. Parker. 1997. *Brock biology of microorganisms*, 8th edition. Prentice Hall.

McKinley, J. P., J. M. Zachara, S. M. Heald, J. K. Fredrickson, C. X. Liu, D. W. Kennedy, A. Dohnalkova, K. M. Rosso, Y. A. Gorby, S. C. Smith, and R. K. Kukkadapu. 2002. The reductive immobilization of pertechnetate by bio-reduced sediments. *AGU Fall Meeting Abstracts*.

Michalsen, M. M., B.A. Goodman, S.D. Kelly, K.M. Kemner, J.P. McKinley, J.W. Stucki, and J.D. Istok. 2006. Uranium and Technetium Bio-Immobilization in Intermediate-Scale Physical Models of an In Situ Bio-Barrier. *Environmental Science & Technology*, 40(22): 7048-7053.

Michalsen, M.M., A. Peacock, A. Spain, A. Smithgal, D. White, Y.Sanchez-Rosario, L. Krumholz, J. Istok. 2007. Sediment Microbial Community Shifts Correlate with Geochemistry in Model Bio-Barrier for Uranium and Technetium Removal from Groundwater. *Applied Environmental Microbiology* (In Press).

Michalsen, M.M., A. Peacock, A. Spain, A. Smithgal, D. White, Y.Sanchez-Rosario, L. Krumholz, J. Istok. 2007. Uranium and technetium transport in acidic groundwater during biostimulation. *Applied Environmental Microbiology* (In Review).

- Mikell, A. T., T. J. Phelps, and D. C. White. 1986. Phospholipids to monitor microbial ecology in anaerobic digesters, p. 413-444. In W. H. S. a. J. R. Frank (ed.), *Methane from Biomass, a Systems Approach*. Elsevier Publishing, New York.
- Mikola, j. and H. Setälä. 1998. Relating species diversity to ecosystem functioning: mechanistic backgrounds and experimental approach with a decomposer food web. *Oikos*, 83, p. 180-194.
- Mohanty, S., B. Kollah, D. Hedrick, A. Peacock, and E. Roden. 2007. Biogeochemical processes and microbial community structure in ethanol-stimulated subsurface sediments. Manuscript in preparation.
- Moore, L. V. H. B., D. M.; Moore, W. E. C. 1994. Comparative distribution and taxonomic value of cellular fatty acids in thirty-three genera of anaerobic Gram-negative bacteria. *Int. J. Syst. Bacteriol.* 44:338-347.
- Mosey, F.E. and X.A. Fernandes. 1989. Patterns of hydrogen in biogas from the anaerobic digestion of milk-sugars. *Water Science and Technology*, 21, p. 187-196.
- Muller, A.K., K. Westergaard, S. Christensen, and S.J. Sørensen. 2002. The diversity and function of soil microbial communities exposed to different disturbances. *Microbial Ecology*, 44: 49-58.
- North, N.N, S.L. Dollhopf, L. Petrie, J.D. Istok, D.L. Balkwill, and J.E. Kostka. 2004. A cultivation-independent investigation of microbial communities during in situ biostimulation of subsurface sediment co-contaminated with uranium and nitrate. *Applied and Environmental Microbiology*, Vol. 70, No. 8, pp: 4911-4920.

- Nuclear Energy Agency, Organization for Economic Co-Operation and Development. 2003. Chemical thermodynamics 5. Update on the chemical thermodynamics of uranium, neptunium, plutonium, americium, and technetium. Elsevier.
- Nützmann, G., P. Viotti, and P. Aagaard. 2005. Consequences of different kinetic approaches for simulation of microbial degradation on contaminant plume development (Chapter 9). In: Reactive Transport in Soil and Groundwater: Processes and Models, Springer, Berlin.
- O'Loughlin, E. J., S. D. Kelly, R. E. Cook, R. Csencsits, and K. M. Kemner. 2003. Reduction of Uranium(VI) by mixed iron(II)/iron(III) hydroxide (green rust): Formation of UO₂ nanoparticles. *Environmental Science & Technology* 37:721-727.
- Ortiz-Bernad, I., R.T. Anderson, H.A. Vrionis, and D.R. Lovley. 2004. Vanadium respiration by *Geobacter metallireducens*: novel strategy for in situ removal of vanadium from groundwater. *Applied and Environmental Microbiology*, 70:3091-3095.
- Park, J., R. A. Sanford, and C. M. Bethke. 2006. Geochemical and microbiological zonation of the Middendorf aquifer, South Carolina. *Chemical Geology* 230: 88 – 104).
- Payne, R. B., D. A. Gentry, B. J. Rapp-Giles, L. Casalot, and J. D. Wall. 2002. Uranium reduction by *Desulfovibrio desulfuricans* strain G20 and a cytochrome c₃ mutant. *Applied and Environmental Microbiology* 68:3129-3132.
- Pedersen, K. 1993. The deep subterranean biosphere. *Earth-Sci Rev*, 34, p. 243-260
- Petrie, L., N.N. North, S.L. Dollhopf, D.L. Balkwill, and J.E. Kostka. 2003. Enumeration and characterization of iron(III)-reducing microbial communities from acidic subsurface sediments contaminated with uranium(VI). *Applied and Environmental Microbiology*, 69(12):7467-79.

- Postma D. and R. Jakobsen. 1996. Redox zonation: equilibrium constraints on the Fe(III)/SO₄-reduction interface. *Geochimica et Cosmochimica Acta* 60, 3169-3175.
- Reeburgh, W.S. 1983. Rates of biogeochemical processes in anoxic sediments. *Ann. Rev. Earth Planet Sci.* 11, p. 269-298.
- Reed, J.L. and V. O. Palsson. 2003. Thirteen years of building constraint-based in silico models of *Escherichia coli*. *Journal of Bacteriology*, 185(9), p. 2692-2699.
- Rittmann, B.E. and P.L. McCarty. 2001. *Environmental biotechnology: Principles and applications*. McGraw Hill, Boston. 754 p.
- Roughgarden, J. R. M. May, and S.A. Levin (eds.). 1989. *Perspectives in Ecological Theory*. Princeton University Press. 375 p.
- Royer, R.A., B.A. Dempsey, B-H. Jeon, and W.D. Burgos. 2004. Inhibition of biological reductive dissolution of hematite by ferrous iron. *Environmental Science & Technology*, 38, 187-193.
- Savinell, J.M. and B.O. Palsson. 1992. Optimal selection of metabolic fluxes for in vivo measurement. I. Development of mathematical models. *J. Theoretical Biology* 155:201-214.
- Schilling, C.H., J.S. Edwards, and B.O. Palsson. 1999. Towards metabolic phenomics: analysis of genomic data using flux balances. *Biotech. Prog.* 15:288-295.
- Schink, B. 1997. Energetics of syntrophic cooperation in methanogenic degradation, *Microbiology and Molecular Biology Reviews*, 61, p. 262-280.
- Schirmer, M., J.F. Barker, B.J. Butler, and E.O. Frind. 2003. Application of lab derived kinetic biodegradation parameters at the field scale. EGS - AGU - EUG Joint Assembly, Abstracts from the meeting held in Nice, France, 6 - 11 April 2003, abstract No. 12227.

- Scott, M.J., J.J. Morgan. 1990. Energetics and conservative properties of redox systems. ACS Symp. Ser. 416; 779-781.
- Seitz, H.J., B. Schink, N. Pfennig, R. Conrad. 1990a. Energetics of syntrophic ethanol oxidation in defined chemostat cocultures. 1. Energy requirement for H₂ production and H₂ oxidation. Arch. Microbiol. 155, p. 82-88.
- Seitz, H.J., B. Schink, N. Pfennig, R. Conrad. 1990b. Energetics of syntrophic ethanol oxidation in defined chemostat cocultures. 2. Energy sharing in biomass production Arch. Microbiol. 155, p. 89-93.
- Senko, J.M., Mohamed, Y., T.A. Dewers and L.R. Krumholz. 2005a. A Role for Fe(III) minerals in nitrate-dependent microbial U(IV) oxidation. Environmental Science & Technology, 39(8); 2529-2536.
- Senko, J.M., T.A. Dewers and L.R. Krumholz. 2005b. The effect of the form of Fe(II) and oxidation rate on microbial nitrate-dependent Fe(III) mineralogy. Appl. Env. Microbiol. 71(11):7172-7177.
- Smith, D.P. and P.L. McCarty. 1990. Factors governing methane fluctuations following shock loading of digesters. J. Water Pollution Control Federation, 62, p. 58-64.
- Stumm, W. and J.J. Morgan. 1981. Aquatic chemistry 2nd edition. John Wiley & Sns.
- Thauer, R.K., K. Jungermann, and K. Decker. 1977. Energy conservation in chemotrophic anaerobic bacteria. Bacteriological Reviews, 41(1), p. 1800-180.
- Tilman, D. 1982. Resource competition and community structure. Princeton University Press, Princeton, NJ.

- Van Capellen, P. and Y. Wang. 1996. Cycling of iron and manganese in surface sediments: A general theory for the coupled transport and reaction of carbon, oxygen, nitrogen, sulfur, iron, and manganese. *American Journal of Science*, Vol. 296: 107-243.
- Vrionis, Helen A., Robert T. Anderson, Irene Ortiz-Bernad, Kathleen R. O'Neill, Charles, T. Resch, Aaron D. Peacock, Richard Dayvault, David C. White, Philip E. Long, and Derek R. Lovley. 2005 Microbiological and Geochemical Heterogeneity in an In Situ Uranium Bioremediation Field Site. *Applied Environmental Microbiology*, 71, No. 10, p. 6308-6318,
- Vroblesky D. A. and F.H. Chapelle. 1994. Temporal and spatial changes of terminal electron-accepting processes in a petroleum hydrocarbon-contaminated aquifer and the significance for contaminant bioremediation. *Water Resources Research* 30(5), 1561-1570.
- Wardle, D.A. and K.E. Giller. 1996. The quest for a contemporary ecological dimension to soil biology. *Soil Biol Biochem*, 28, p. 1549-1554.
- Wielinga, Bruce, B.C. Bostick, C. M. Hansel, R.F. Rosenzweig, S.E. Fendorf. 2000. Inhibition of Bacterially Prompted Uranium Reduction: Ferric (Hydroxides as Competitive Electron Acceptors. *Environmental Science & Technology* 34:2190-2195.
- Wildung, R. E., Y. A. Gorby, K. M. Krupka, N. J. Hess, S. W. Li, A. E. Plymale, J. P. McKinley, and J. K. Fredrickson. 2000. Effect of electron donor and solution chemistry on products of dissimilatory reduction of technetium by *Shewanella putrefaciens*. *Applied Environmental Microbiology*, 66:2451-2460.
- Williams, S.T. 1985. Oligotrophy in soil: fact or fiction ? In *Bacteria in the Natural Environment: the Effect of Nutrient Conditions*, M. Fletcher and G. Floodgate (eds), pp. 81-110. Academic Press, London.

- Wu, Q, R.A. Sanford, and F. E. Löffler. 2006. Uranium(VI) Reduction by *Anaeromyxobacter dehalogenans* Strain 2CP-C. *Applied Environmental Microbiology*, 72:3608-3614.
- Wu, W-M. J. Carley, M. Fienen, T. Mehlhorn, K. Lowe, J. Nyman, J. Luo, M. E. Gentile, R. Rajan, D. Wagner, R. F. Hickey, B. Gu, D. Watson, O. A. Cirpka, P. K. Kitanidis, P. M. Jardine, and C. S. Criddle. 2006a. Pilot-Scale in Situ Bioremediation of Uranium in a Highly Contaminated Aquifer. 1. Conditioning of a Treatment Zone. *Environmental Science & Technology*, 40 (12), 3978 -3985
- Wu, W-M. J. Carley, T. Gentry, M. A. Ginder-Vogel, M. Fienen, T. Mehlhorn, H. Yan, S. Carroll, M. N. Pace, J. Nyman, J. Luo, M. E. Gentile, M. W. Fields, R. F. Hickey, B. Gu, D. Watson, O. A. Cirpka, J. Zhou, S. Fendorf, P. K. Kitanidis, P. M. Jardine, and C. S. Criddle. 2006b. Pilot-Scale in Situ Bioremediation of Uranium in a Highly Contaminated Aquifer. 2. Reduction of U(VI) and Geochemical Control of U(VI) Bioavailability. *Environ. Sci. Technol.*, 40 (12), 3986 -3995.
- Xia, B. C., D. S. Treves, J. Z. Zhou, and J. M. Tiedje. 2001. Soil microbial community diversity and driving mechanisms. *Progress in Natural Science* 11:818-824.
- Yabusaki, S.B., Y. Fang, P.E. Long, C.T. Resch, A.D., Peacock, J. Komlos, P.R. Jaffe, S.J. Morrison, P.D. Dayvault, D.C. White, R.T. Anderson. 2007. Uranium removal from groundwater via in situ biostimulation: field-scale modeling of transport and biological processes. Accepted with revision, *Journal of Contaminant Hydrology*.
- Zachara, J. M., J. K. Fredrickson, S. C. Smith, and P. L. Gassman. 2001. Solubilization of Fe(III) oxide-bound trace metals by a dissimilatory Fe(III) reducing bacterium. *Geochimica et Cosmochimica Acta* 65:75-93.

- Zachara, J. M., J. K. Fredrickson, S. M. Li, D. W. Kennedy, S. C. Smith, and P. L. Gassman. 1998. Bacterial reduction of crystalline Fe^{3+} oxides in single phase suspensions and subsurface materials. *American Mineralogist* 83:1426-1443.
- Zhou, J. Z., B. C. Xia, D. S. Treves, L. Y. Wu, T. L. Marsh, R. V. O'Neill, A. V. Palumbo, and J. M. Tiedje. 2002. Spatial and resource factors influencing high microbial diversity in soil. *Applied and Environmental Microbiology* 68:326-334.

energy (ΔG^0_r), logK, and growth equation stoichiometries used in simulations.

	Acceptor	Donor		ΔG°_r	Growth Equation																		
Group	Half-Reaction	Half-Reaction	YDx	(kJ/mol)	logK																		
1	O ₂ /CO ₂	Ethanol/CO ₂	0.56	3318	-581	-4.9	H ⁺	-7.5	H ₂ O	-3.9	HCO ₃ ⁻	1.0	NH ₄ ⁺	8.4	O ₂ (aq)	4.5	ethanol						
2		Acetate/CO ₂	0.41	2731	-478	-2.1	H ⁺	-3.0	H ₂ O	-7.2	HCO ₃ ⁻	1.0	NH ₄ ⁺	7.2	O ₂ (aq)	6.1	CH ₃ COO ⁻						
3		Ethanol/Acetate	0.14	5309	-930	-13.4	H ⁺	-20.4	H ₂ O	5.0	HCO ₃ ⁻	1.0	NH ₄ ⁺	12.4	O ₂ (aq)	-17.4	CH ₃ COO ⁻	17.4	ethanol				
4		H ₂ /H ⁺	0.13	7082	-1241	4.0	H ⁺	38.6	H ₂ (aq)	-41.6	H ₂ O	5.0	HCO ₃ ⁻	1.0	NH ₄ ⁺	14.3	O ₂ (aq)						
5		CH ₄ /CO ₂	0.55	5019	-879	-5.0	H ⁺	-12.0	H ₂ O	-4.0	HCO ₃ ⁻	1.0	NH ₄ ⁺	13.0	O ₂ (aq)	9.0	CH ₄ (aq)						
6	NO ₃ ⁻ /N ₂	Ethanol/CO ₂	0.27	9037	-1583	3.7	H ⁺	-21.4	H ₂ O	-13.5	HCO ₃ ⁻	-9.1	N ₂ (aq)	1.0	NH ₄ ⁺	18.2	NO ₃ ⁻	9.3	ethanol				
7		Acetate/CO ₂	0.41	2605	-456	3.7	H ⁺	-5.9	H ₂ O	-7.2	HCO ₃ ⁻	-2.9	N ₂ (aq)	1.0	NH ₄ ⁺	5.8	NO ₃ ⁻	6.1	CH ₃ COO ⁻				
8		Ethanol/Acetate	0.29	1344	-236	-1.7	H ⁺	-13.0	H ₂ O	5.0	HCO ₃ ⁻	-1.4	N ₂ (aq)	1.0	NH ₄ ⁺	2.9	NO ₃ ⁻	-8.6	CH ₃ COO ⁻	8.6	ethanol		
9		H ₂ /H ⁺	0.17	4805	-842	12.0	H ⁺	30.0	H ₂ (aq)	-37.0	H ₂ O	5.0	HCO ₃ ⁻	-4.0	N ₂ (aq)	1.0	NH ₄ ⁺	8.0	NO ₃ ⁻				
10	Fe ³⁺ /Fe ²⁺	Acetate/CO ₂	0.12	8153	-1428	-150.2	Fe ²⁺	150.2	Fe ³⁺	-167.4	H ⁺	72.1	H ₂ O	-37.5	HCO ₃ ⁻	1.0	NH ₄ ⁺	21.3	CH ₃ COO ⁻				
11		Ethanol/Acetate	0.13	3393	-594	-57.7	Fe ²⁺	57.7	Fe ³⁺	-73.1	H ⁺	6.4	H ₂ O	5.0	HCO ₃ ⁻	1.0	NH ₄ ⁺	-19.4	CH ₃ COO ⁻	19.4	ethanol		
12		H ₂ /H ⁺	0.07	8593	-1505	-114.8	Fe ²⁺	114.8	Fe ³⁺	-110.8	H ⁺	67.4	H ₂ (aq)	-13.0	H ₂ O	5.0	HCO ₃ ⁻	1.0	NH ₄ ⁺				
13	SO ₄ ²⁻ /HS ⁻	Acetate/CO ₂	0.10	787	-138	1.5	H ⁺	-3.0	H ₂ O	-44.9	HCO ₃ ⁻	-22.5	HS ⁻	1.0	NH ₄ ⁺	22.5	SO ₄ ²⁻	25.0	CH ₃ COO ⁻				
14		Ethanol/Acetate	0.04	2692	-472	-31.8	H ⁺	-69.5	H ₂ O	5.0	HCO ₃ ⁻	-30.8	HS ⁻	1.0	NH ₄ ⁺	30.8	SO ₄ ²⁻	-66.5	CH ₃ COO ⁻	66.5	ethanol		
15		H ₂ /H ⁺	0.07	3415	-598	21.4	H ⁺	79.6	H ₂ (aq)	-82.6	H ₂ O	5.0	HCO ₃ ⁻	-17.4	HS ⁻	1.0	NH ₄ ⁺	17.4	SO ₄ ²⁻				
16	MnO ₄ ²⁻ /Mn ²⁺	Acetate/CO ₂	0.12	22342	-3914	134.0	H ⁺	-78.7	H ₂ O	-37.9	HCO ₃ ⁻	-37.9	Mn ²⁺	37.9	MnO ₄ ²⁻	1.0	NH ₄ ⁺	21.4	CH ₃ COO ⁻				
17		Ethanol/Acetate	0.29	2128	-373	10.1	H ⁺	-19.1	H ₂ O	5.0	HCO ₃ ⁻	-3.7	Mn ²⁺	3.7	MnO ₄ ²⁻	1.0	NH ₄ ⁺	-8.7	CH ₃ COO ⁻	8.7	ethanol		
18		H ₂ /H ⁺	0.15	8061	-1412	51.7	H ⁺	33.9	H ₂ (aq)	-60.7	H ₂ O	5.0	HCO ₃ ⁻	-11.9	Mn ²⁺	11.9	MnO ₄ ²⁻	1.0	NH ₄ ⁺				
19	CO ₂ /CH ₄	Acetate/CO ₂	0.02	1194	-209	1.5	H ⁺	98.2	H ₂ O	-101.2	HCO ₃ ⁻	1.0	NH ₄ ⁺	103.7	CH ₃ COO ⁻	-101.2	CH ₄ (aq)						
20		H ₂ /H ⁺	0.02	12926	-2265	84.9	H ⁺	333.5	H ₂ (aq)	-255.6	H ₂ O	85.9	HCO ₃ ⁻	1.0	NH ₄ ⁺	-80.9	CH ₄ (aq)						
21	H ⁺ /H ₂	Acetate/CO ₂	0.11	-1616	283	-7.7	H ⁺	33.7	H ₂ O	-18.4	HCO ₃ ⁻	1.0	NH ₄ ⁺	-36.7	H ₂ (aq)	11.7	CH ₃ COO ⁻						
22		Ethanol/Acetate	0.01	-24671	4322	-496.0	H ⁺	487.0	H ₂ O	5.0	HCO ₃ ⁻	1.0	NH ₄ ⁺	-990.0	H ₂ (aq)	-500.0	CH ₃ COO ⁻	500.0	ethanol				
23	UO ₂ ²⁺ /U ⁴⁺	Acetate/CO ₂	0.22	-58	-230	66.4	H ⁺	-40.1	H ₂ O	-18.5	HCO ₃ ⁻	1.0	NH ₄ ⁺	11.8	CH ₃ COO ⁻	-37.1	U ⁴⁺	37.1	UO ₂ ²⁺				
24		Ethanol/Acetate	0.19	-49	-125	23.5	H ⁺	-32.5	H ₂ O	5.0	HCO ₃ ⁻	1.0	NH ₄ ⁺	-13.2	CH ₃ COO ⁻	13.2	ethanol	-16.4	U ⁴⁺	16.4	UO ₂ ²⁺		
25		H ₂ /H ⁺	0.12	-166	-244	37.4	H ⁺	26.7	H ₂ (aq)	-46.4	H ₂ O	5.0	HCO ₃ ⁻	1.0	NH ₄ ⁺	-16.7	U ⁴⁺	16.7	UO ₂ ²⁺				
26	TcO ₄ ⁻ /TcO ²⁺	Acetate/CO ₂	0.07	12162	-2131	245.2	H ⁺	-142.3	H ₂ O	-69.6	HCO ₃ ⁻	1.0	NH ₄ ⁺	37.3	CH ₃ COO ⁻	92.8	TcO ₄ ⁻	-92.8	TcO ²⁺				
27		Ethanol/Acetate	0.06	7625	-1336	115.2	H ⁺	-124.2	H ₂ O	5.0	HCO ₃ ⁻	1.0	NH ₄ ⁺	-43.7	CH ₃ COO ⁻	43.7	ethanol	51.6	TcO ₄ ⁻	-51.6	TcO ²⁺		
28		H ₂ /H ⁺	0.04	7346	-1287	120.0	H ⁺	68.0	H ₂ (aq)	-129.0	H ₂ O	5.0	HCO ₃ ⁻	1.0	NH ₄ ⁺	38.7	TcO ₄ ⁻	-38.7	TcO ²⁺				

Table 2. Initial geochemical data used in model simulations.

	FRC Area 2	FRC Area 1	Old Rifle
	(mM)	(mM)	(mM)
pH	6.4	3.3	7.3
O₂	0.07	0.10	0.02
NO₃⁻	1.2	100.0	0.1
SO₄²⁻	0.8	0.4	6.4
Iron oxides (assumed to be goethite) (mmol/kg)	306	361	124
Mn oxides (assumed to be pyrolusite) (mmol/kg)	48	22	10
Ca²⁺	3.5	18.0	5.3
Mg²⁺	1.1	8.3	5.4
Al³⁺	-	12.0	-
HCO₃⁻	0.10	0.00	0.10
U	4.9x10⁻³	1.4x10⁻³	5.25 x 10⁻⁴
V	-	-	1.54 x10⁻²
Tc	4.1x10⁻⁷	1.8x10⁻⁵	-
Electron donor	Ethanol	Ethanol	Acetate

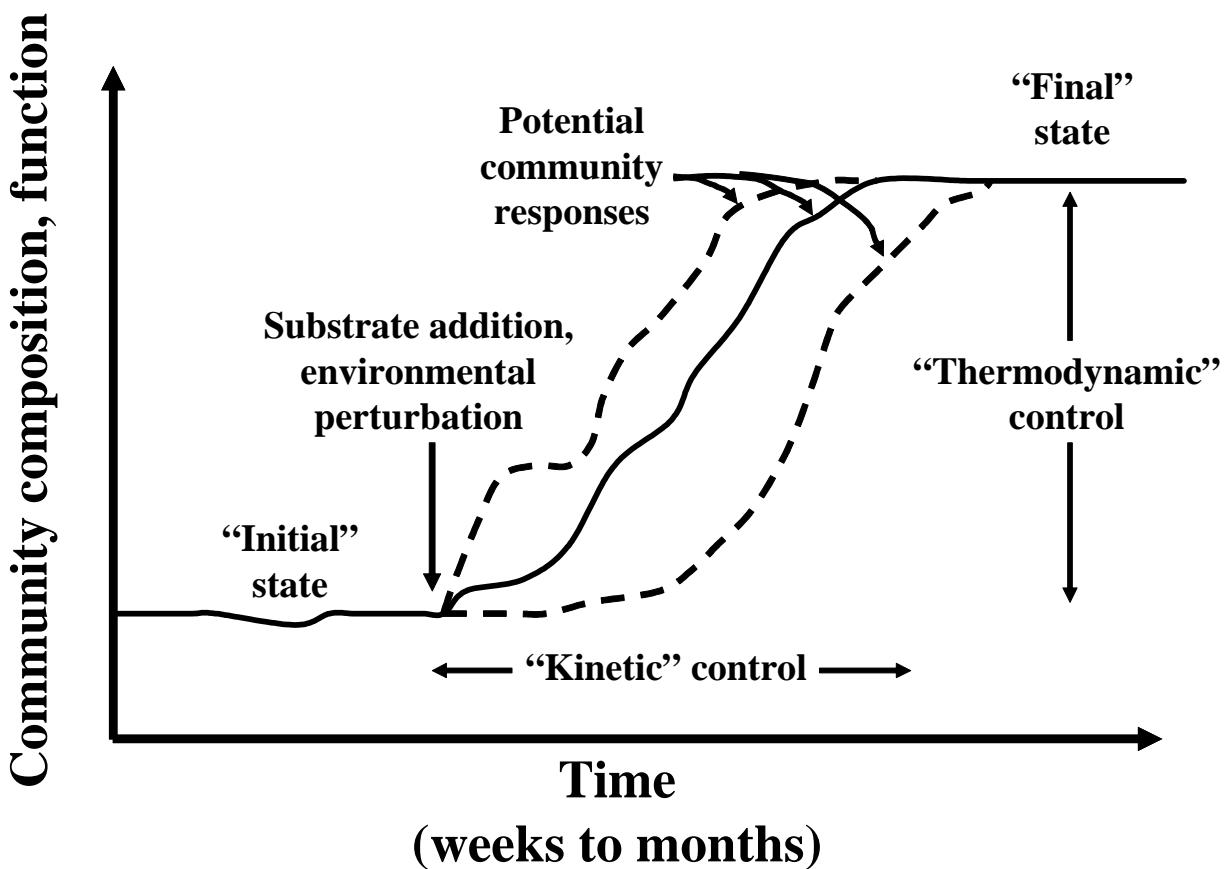


Figure 1 - Hypothetical response of microbial community to substrate addition or environmental perturbation. Kinetic modeling attempts to predict growth as a function of time and other system variables during the period labeled “kinetic control”. This paper describes a modeling approach aimed at predicting microbial growth and resulting change in community composition after growth has ceased (labeled “thermodynamic control”), which is determined by the system-specific coupling between microbial growth and geochemical reactions.

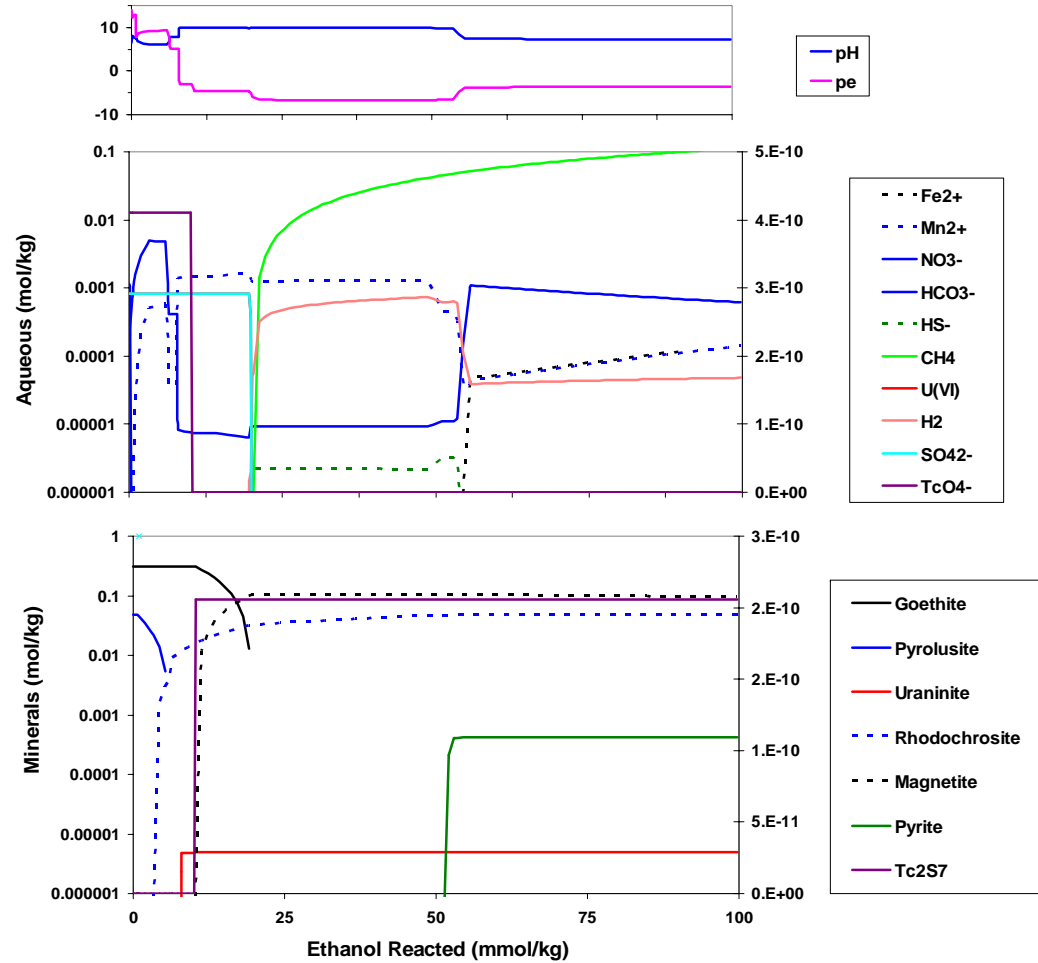
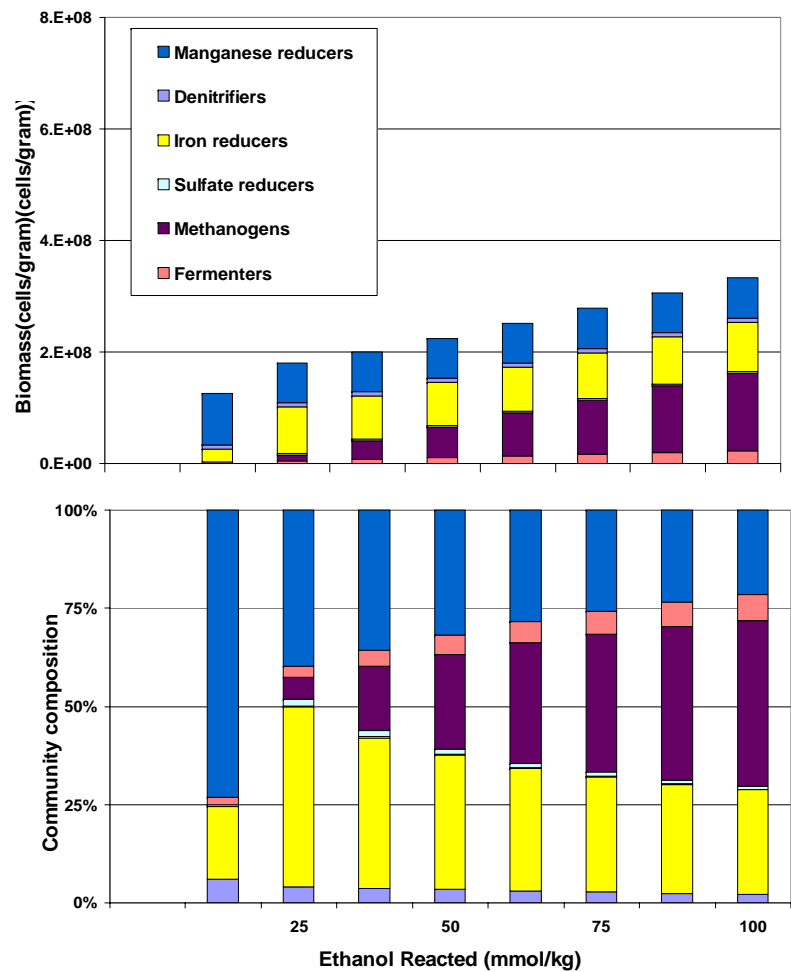


Figure 2 - Batch simulation for FRC Area 2.

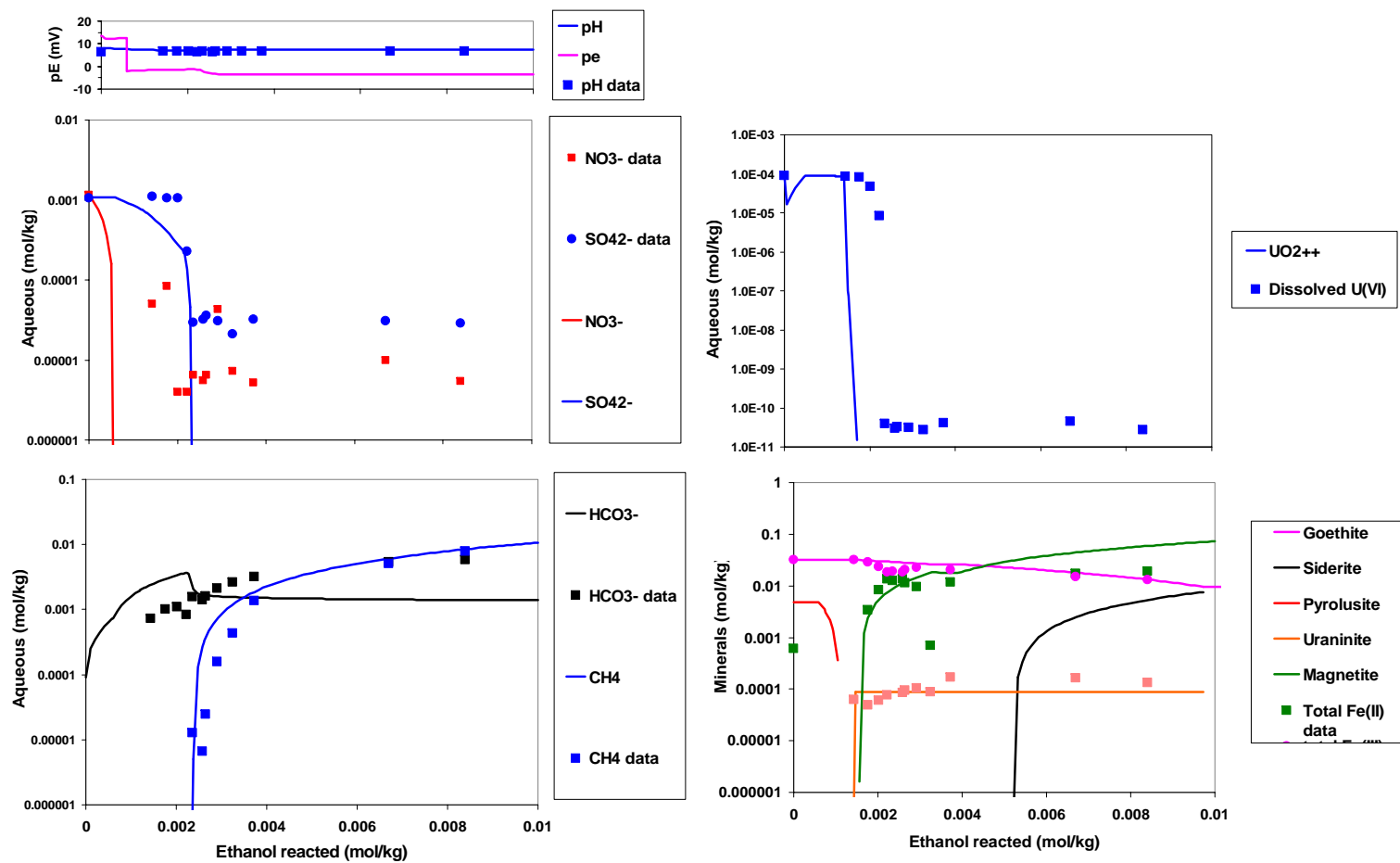


Figure 3 – Comparison of batch simulations with geochemical measurements from laboratory microcosm experiment.

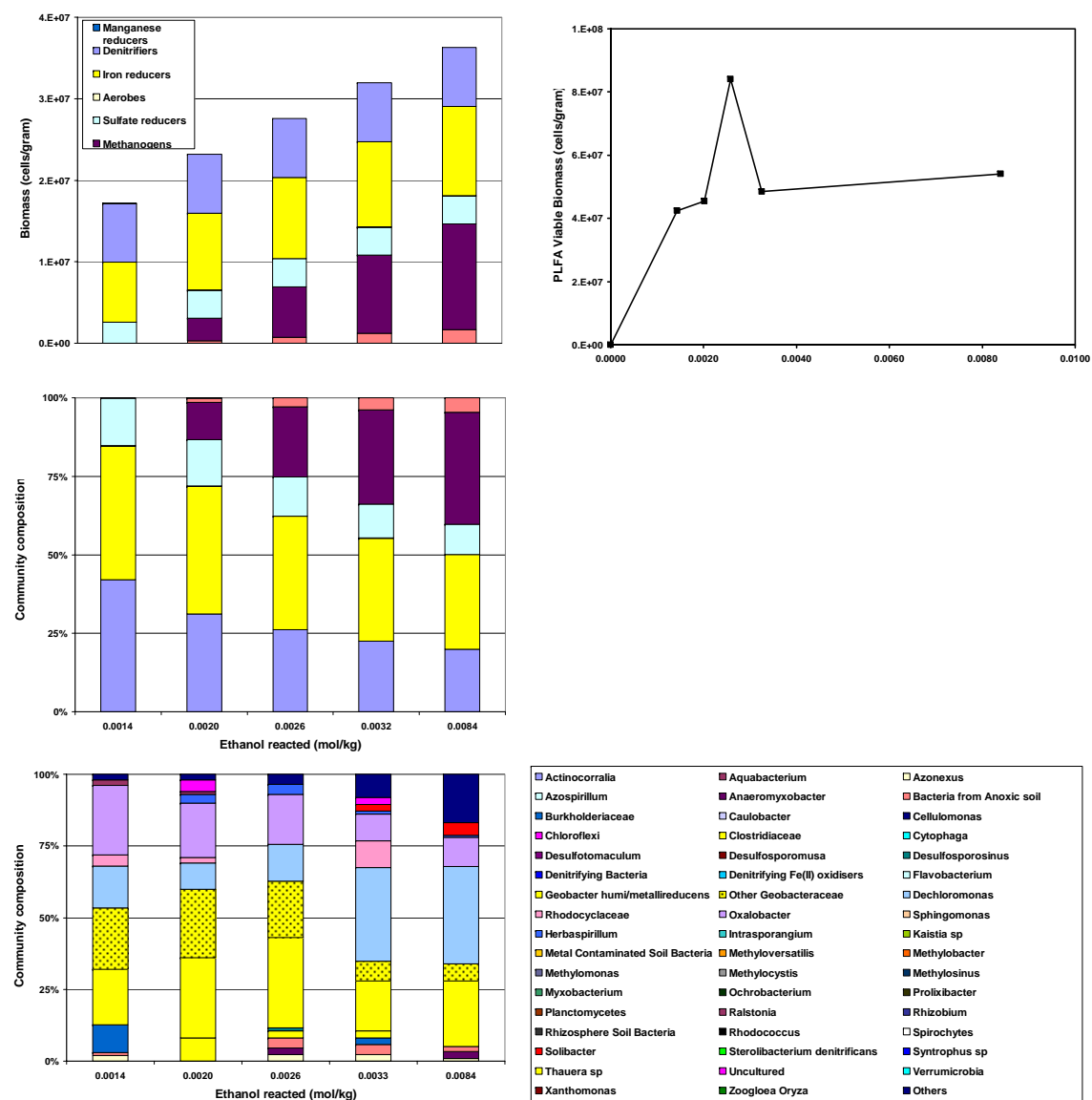


Figure 4 – Comparison of batch simulations for growth and community composition with PLFA biomass and clone library data from laboratory microcosm experiment

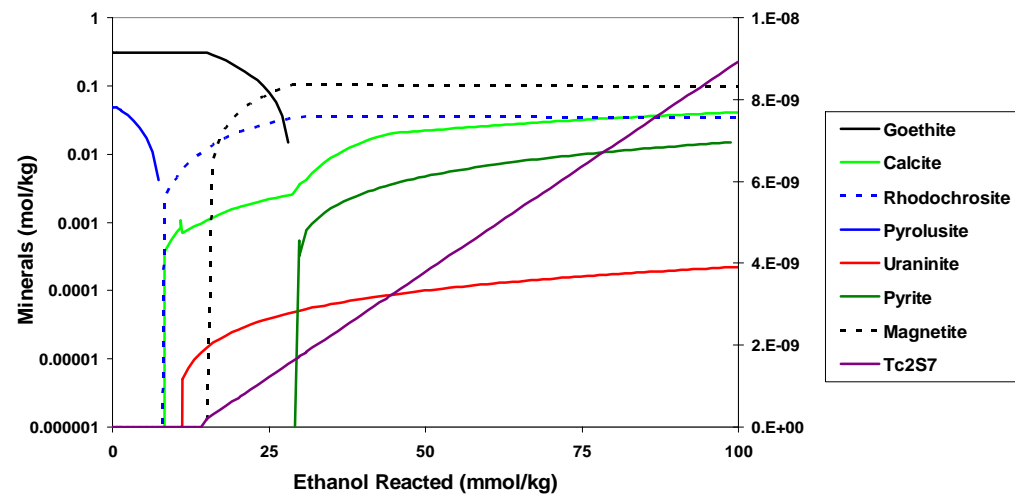
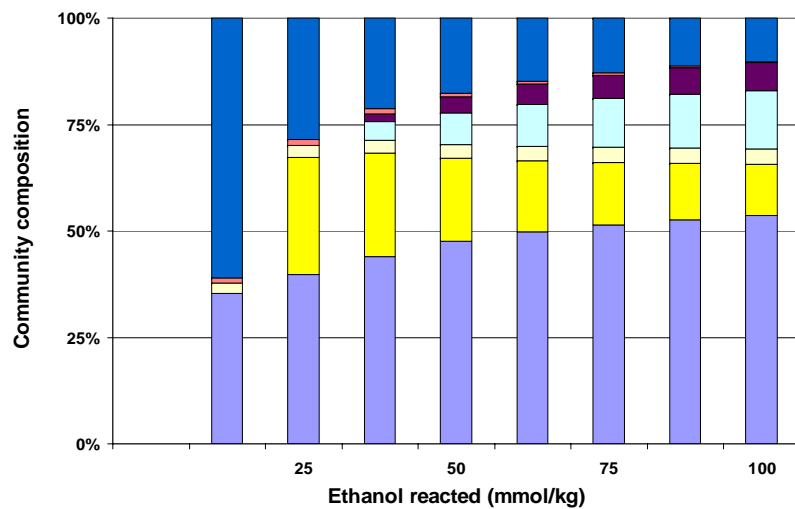
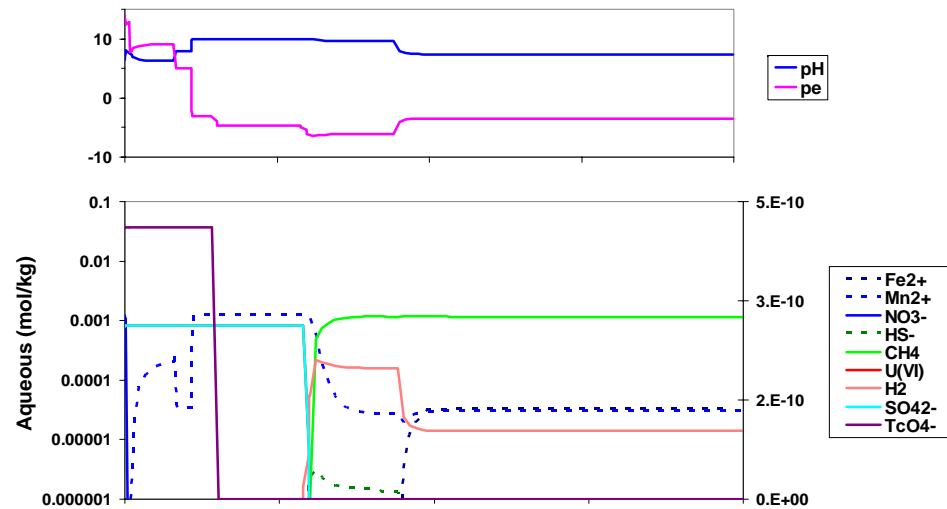
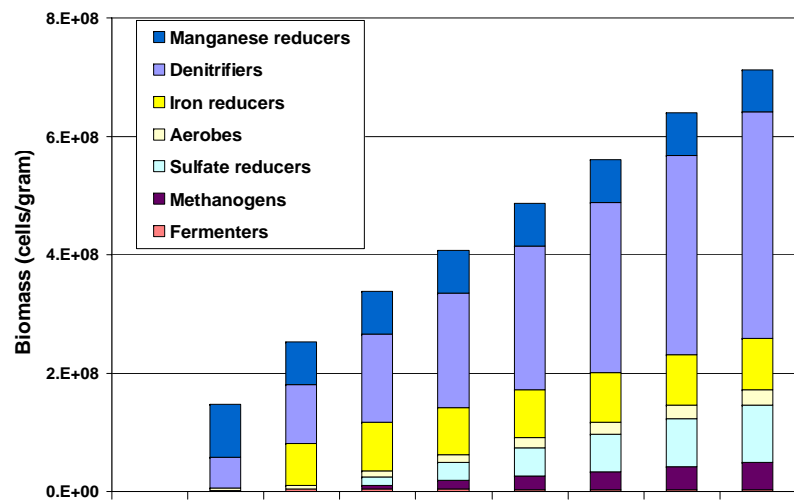


Figure 5 - Flush simulation for FRC Area 2.

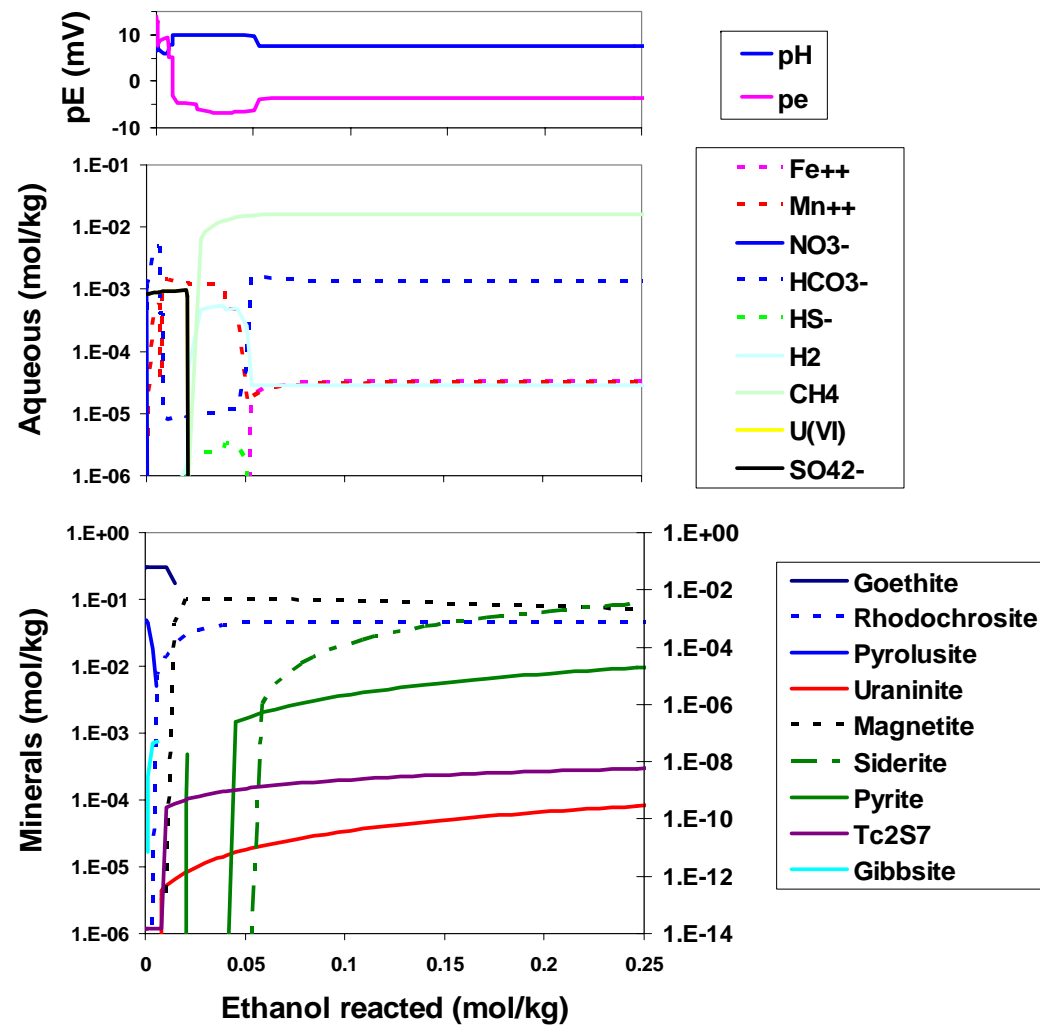


Figure 6 – Simulation of long-term column experiment conducted at FRC Area 2 by Michalsen et al. (2006).

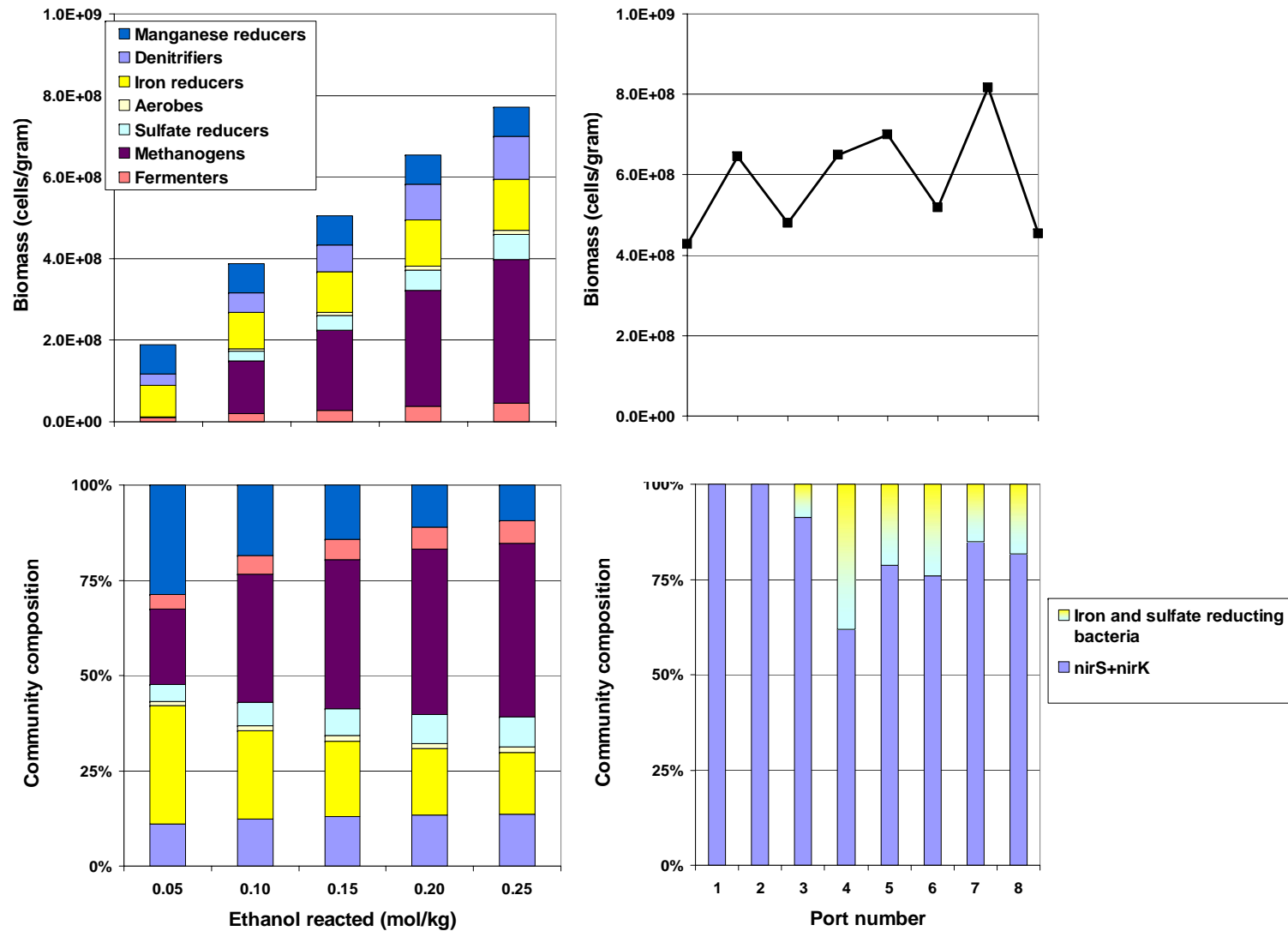


Figure 7 – Comparison of simulated microbial growth and community composition with measured PLFA and Q-PCR from sediment samples collected during long-term column experiment conducted at FRC Area 2 by Michalsen et al. (2006).

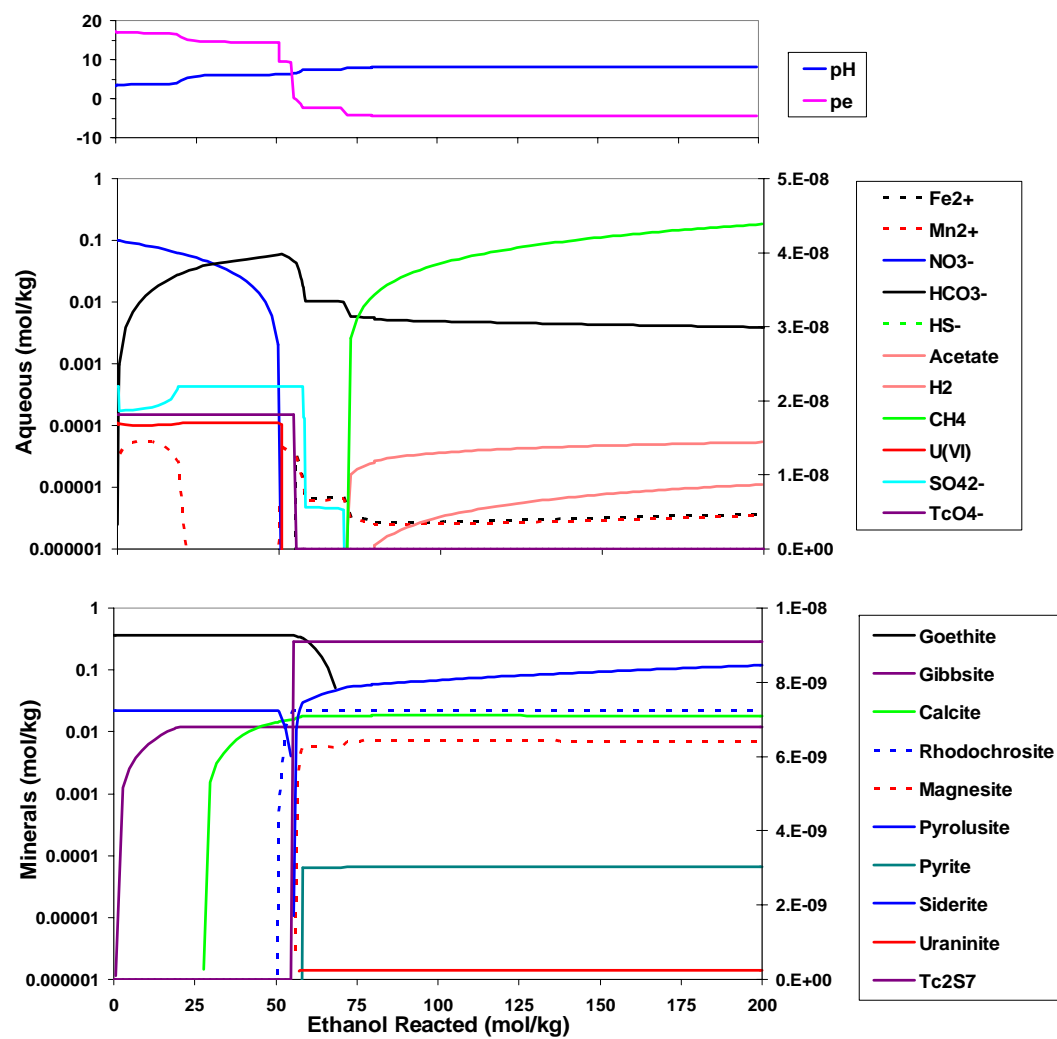
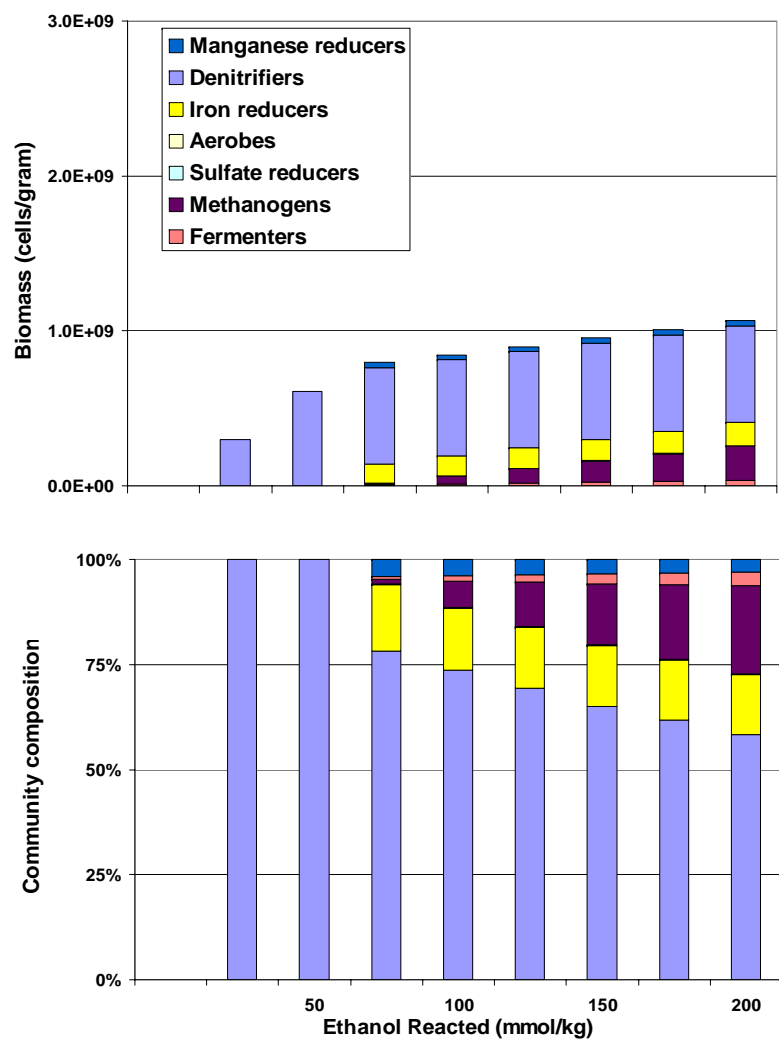


Figure 8 - Batch simulation for FRC Area 1

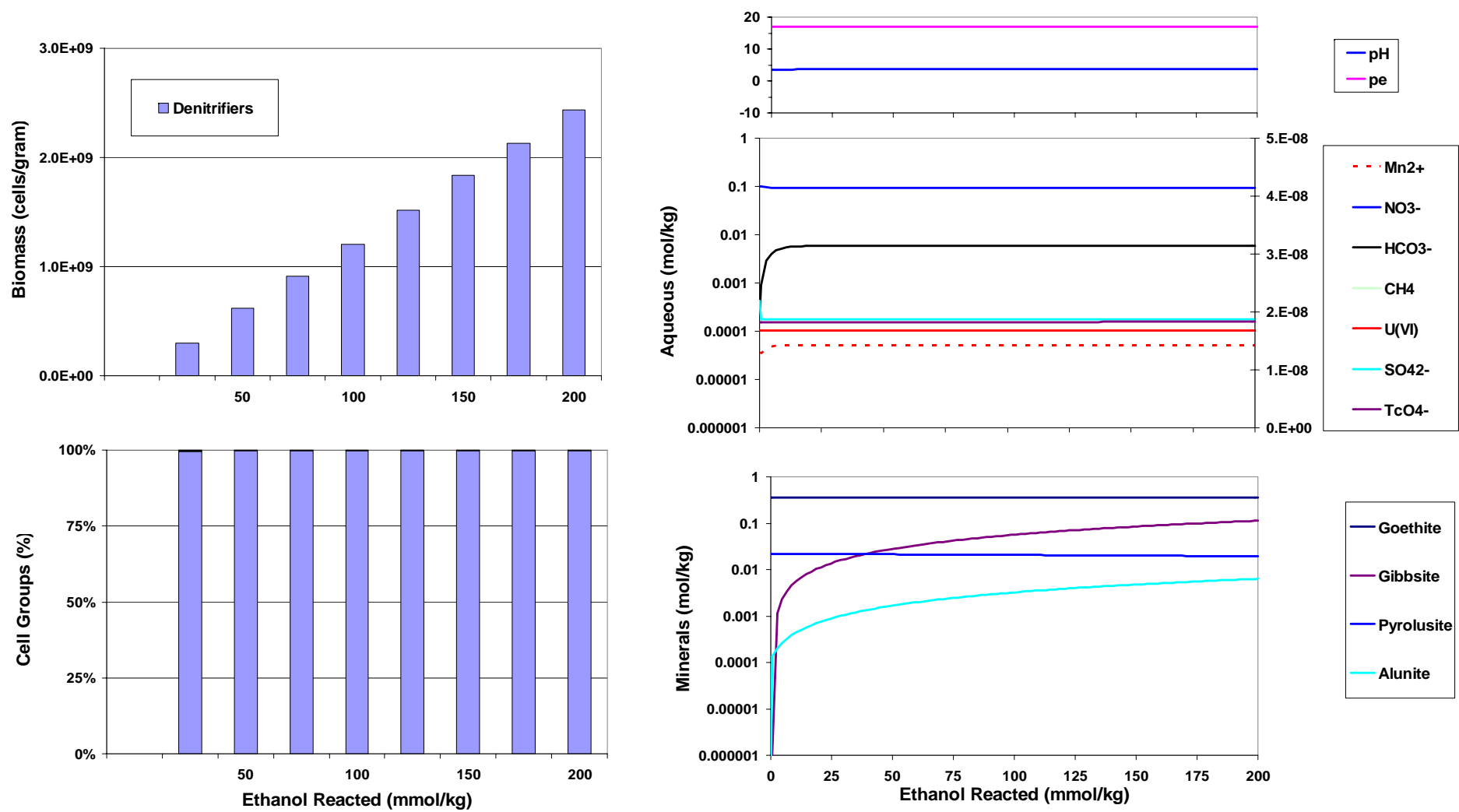


Figure 9 - Flush simulation for FRC Area 1.

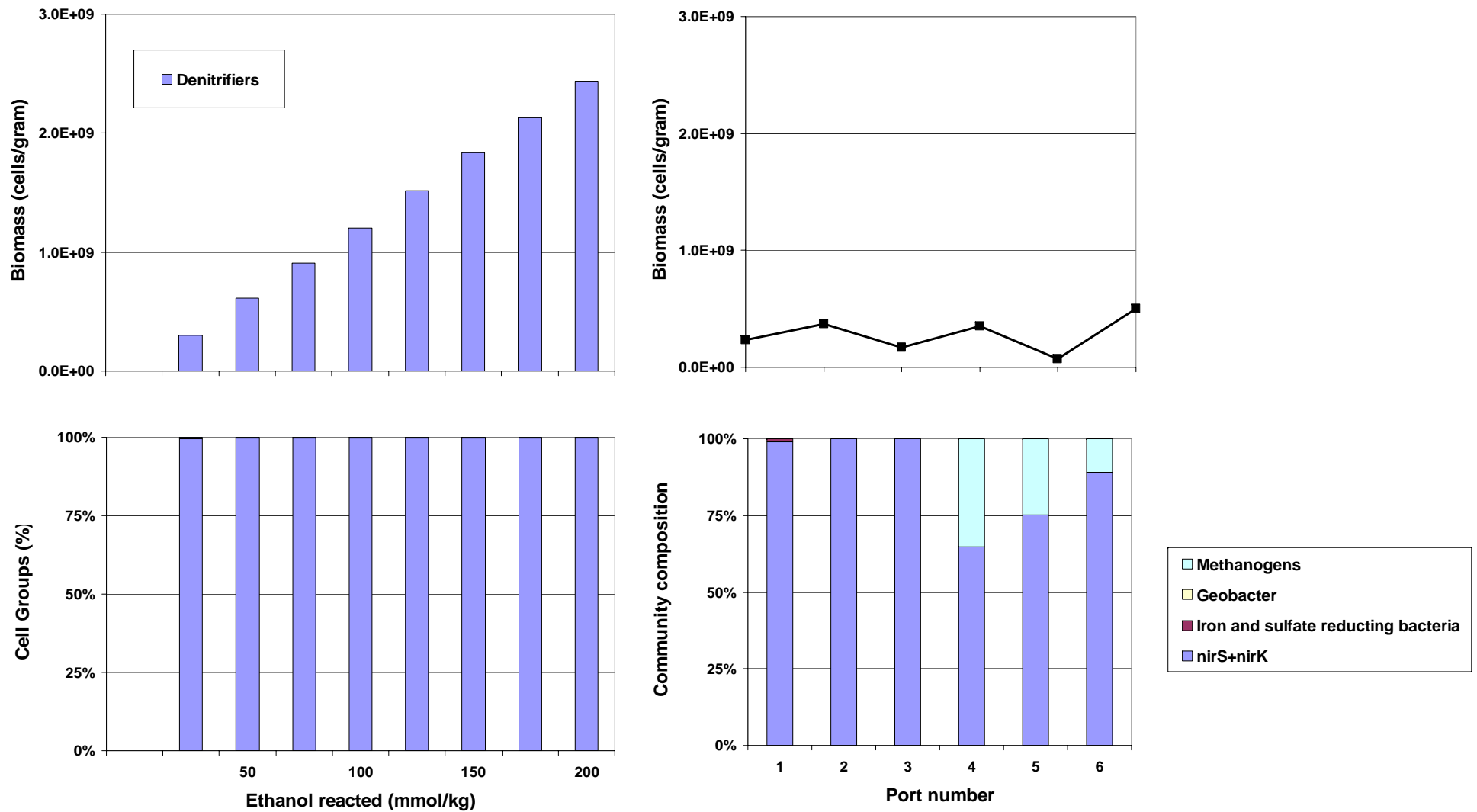


Figure 10 – Comparison of simulated microbial growth and community composition with measured PLFA and Q-PCR from sediment samples collected during long-term column experiment conducted at FRC Area 1 by Michalsen et al. (2006).

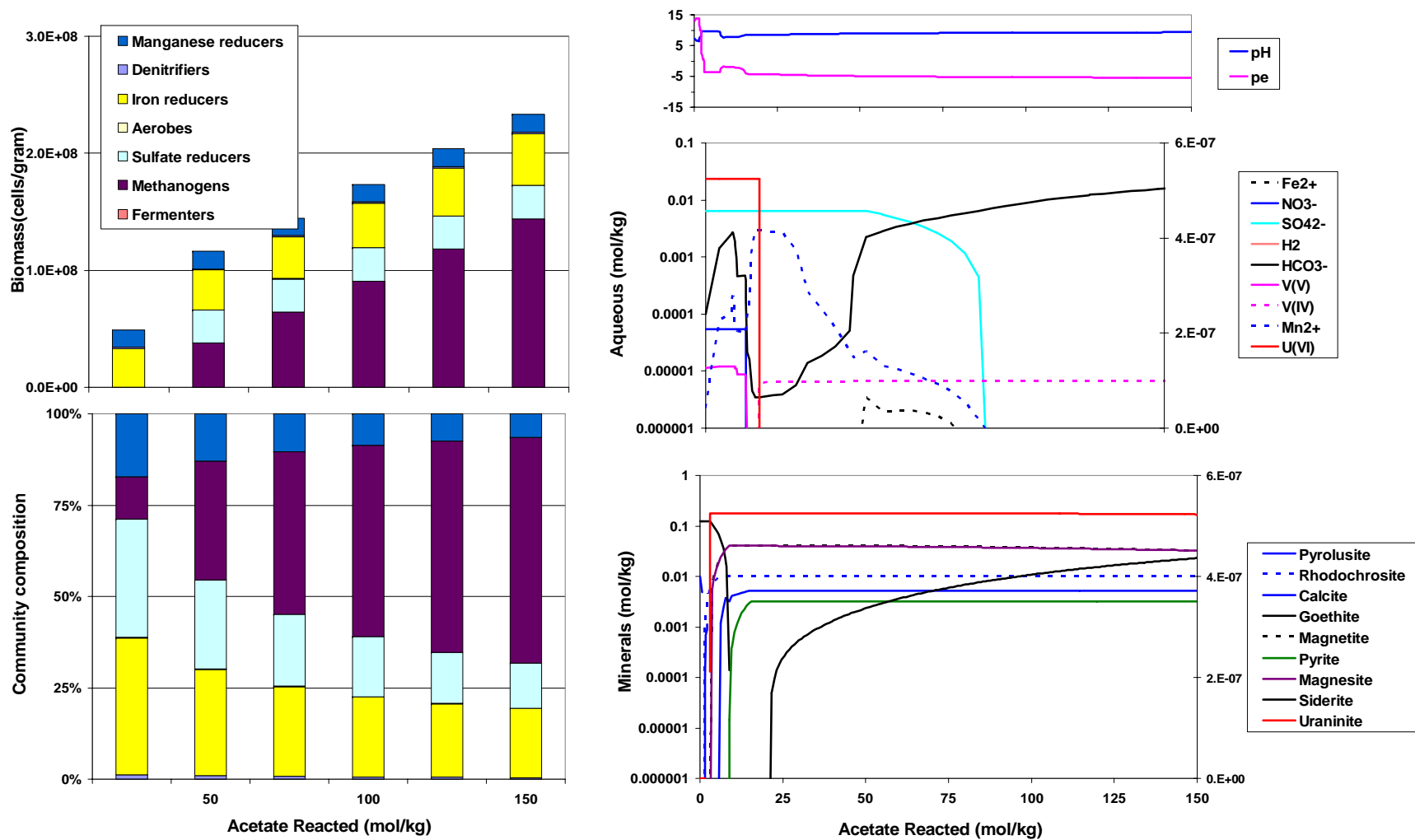


Figure 11 - Batch simulation for Old Rifle.

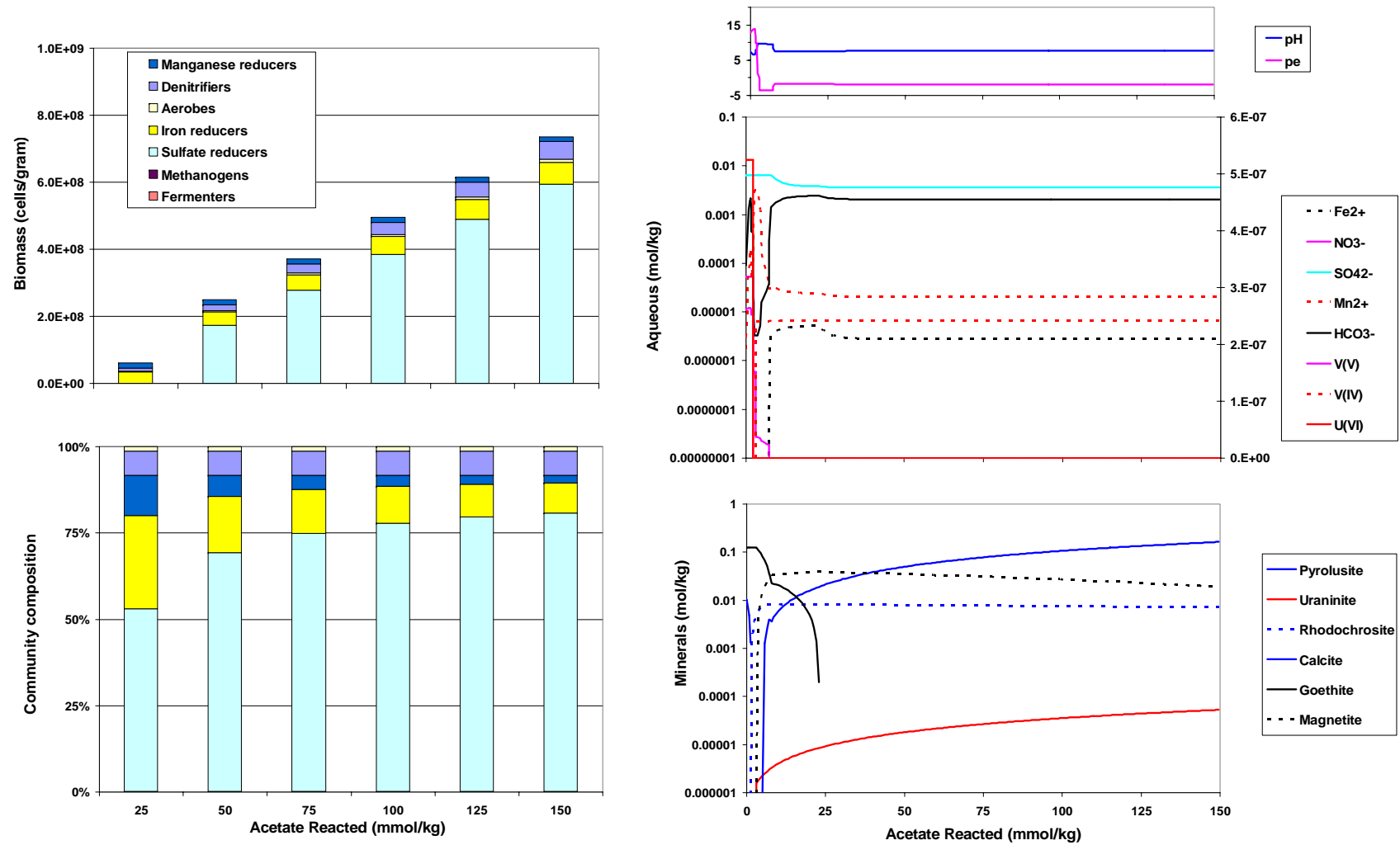


Figure 12 - Flush simulation for Old Rifle.

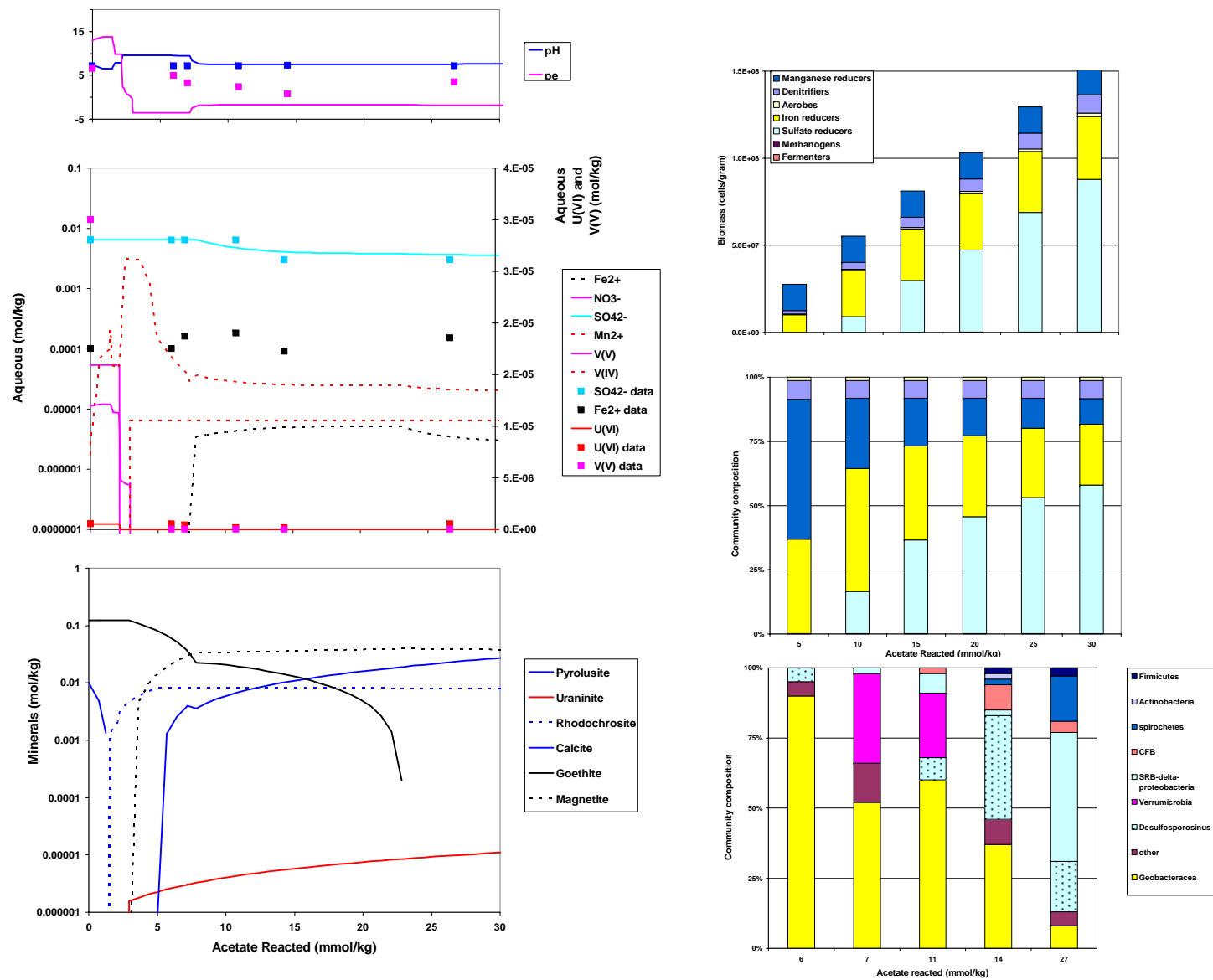


Figure 13- Comparison of flush simulations with geochemical data and clone libraries from natural gradient field experiment at Old Rifle.